



Modelling hail hazard over Italy with ERA5 large-scale variables

Verónica Torralba ^{a,1,*}, Riccardo Hénin ^{a,1,*}, Antonio Cantelli ^{a,b}, Enrico Scoccimarro ^a, Stefano Materia ^a, Agostino Manzato ^c, Silvio Gualdi ^a

^a Climate Simulations and Predictions Division, Fondazione Centro Euro-Mediterraneo sui Cambiamenti Climatici (CMCC), Bologna, Italy

^b Assicurazioni Generali S.p.A., Trieste, Italy

^c Agenzia Regionale Per l'Ambiente (ARPA) Friuli Venezia Giulia – OSMER, Palmanova, Italy



ARTICLE INFO

Keywords:

Hail model
Italy
Genetic algorithm
ERA5
Extremes

ABSTRACT

Hail is a meteorological phenomenon with adverse impacts that affects multiple socio-economic sectors such as agriculture, renewable energy, and insurance. Nevertheless, the understanding of the favourable environmental conditions for hail formation and the models' inadequacy to represent these phenomena have been limited by the scarce temporal and spatial coverage of hail observations. This is a major concern for the mitigation of hail-related risk in sensitive regions such as Italy, which is one of the more hail-prone areas in Europe. In this work, we present a hail model that has been developed to describe the hail hazard over Italy. This model relies on several ERA5 large-scale meteorological variables and convective indices that are combined following the statistical method described in Prein and Holland (2018). The identification of the best set of variables to be used as predictors in the hail model has been performed by a systematic machine learning procedure based on a genetic algorithm. The hail model estimates the hail probability over Italy in the 1979–2020 period, on the ERA5 spatial grid resolution (~30 km). The output of the hail model has been used to characterize the seasonality and long-term variability of hail events in Italy. Furthermore, the categorical verification of the hail probability over the Friuli Venezia Giulia region has revealed that the hail model is able to effectively estimate the hail occurrences in specific Italian regions.

1. Introduction

Hail is a meteorological hazard affecting several industrial sectors (Martius et al., 2018; Changnon et al., 2009). For example, the agricultural industry suffers from the destruction of crops due to large hail stones (Sánchez et al., 1996) which has fostered the development of hail prevention and suppression techniques (Rogna et al., 2021; Rivera et al., 2020). Similarly, the electricity power supply market is impacted by the potential hail-related erosion of wind turbines and solar panels and by damages to the systems for electricity transmission (e.g., Teule et al., 2019; Muehleisen et al., 2018; Macdonald et al., 2016). Hence, the hail risk affecting different socio-economic sectors has promoted the increase of products and services offered by the insurance markets to cover hail damages on property goods (e.g., roofs, windows, cars, ...). Furthermore, insurance claims data have also been employed to quantify hail damages and to evaluate the related loss potential (Púčik et al., 2019; Brown et al., 2015).

Hail characteristics proved difficult to have comprehensive and homogeneous long-term observational datasets required for accurately describing and monitoring the hail phenomenon and related impacts

(Mohr et al., 2015b). Hail events are mainly produced by convective storms that have a local extent and a short duration, therefore the standard observational network often is inadequate (e.g., Mohr and Kunz, 2013). In addition, hail formation and growth are reproduced with some degree of uncertainty by numerical models due to the limitation introduced by the microphysics parameterization and convection schemes (Allen et al., 2015). Moreover, the simulation of these processes requires considerable computational resources (Gagne et al., 2017). However, several approaches have already been employed for hail detection. Hail data has been gathered from satellite-derived proxies for overshooting top (Punge et al., 2017), microwave scattering (Laviola et al., 2020), radar reflectivity (Fluck et al., 2021; Nisi et al., 2016) and from ground-based networks of hail pads (e.g., Eccel et al., 2012; Palencia et al., 2009; Dessens and Fraile, 1994) and reports from the insurance industry (Púčik et al., 2019). Although there is a wide variety of data sources, it is still difficult to compare the hail characteristics in different regions. For example, typical synoptic patterns associated with hailstorms have been examined in European regions such as Portugal (Santos and Belo-Pereira, 2019), northeastern

* Corresponding authors.

E-mail addresses: veronica.torralba@cmcc.it (V. Torralba), riccardo.henin@cmcc.it (R. Hénin).

¹ Contributed equally to this work.

Spain (García-Ortega et al., 2011), southwestern France (Merino et al., 2019), Germany (Mohr and Kunz, 2013) and Poland (Czernecki et al., 2019). In this regard, Punge and Kunz (2016) provides a comprehensive review of the different hail statistics and available datasets employed for several European regions.

Despite northern Italy has been identified as one of the regions with the highest hail frequency in Europe (e.g. Púčik et al., 2019; Punge et al., 2017; Mohr et al., 2015b), the number of comprehensive studies assessing hail hazards over Italy is still limited. Due to the absence of a national monitoring network, regional data have been used for the characterization of hail conditions over specific areas of northeastern Italy, as for the Adige river basin (Eccel et al., 2012) or the Friuli Venezia Giulia region (Manzato, 2012; Gaiotti et al., 2003) and in Tuscany (Piani et al., 2005). Furthermore, Baldi et al. (2014) took the first step towards a national hail database by employing the European Severe Storms Laboratory (ESSL) data combined with a linear multi-regression model to estimate the past frequency of hailstorms. However, this work is based on a limited period (2001–2009), hardly representative of the climatology of hail events over Italy.

To overcome the problem of sparse observations, the study of long-term hail variability has been traditionally carried out by using large-scale variables as drivers of the hailstorm formation (Mohr and Kunz, 2013). This is because the hailstorm development can be controlled by large-scale environmental conditions, even if the hail phenomenon has a local influence (Brooks et al., 2003), therefore the link between the large- and local-scale has been already exploited for the development of hail models. Some examples can be found both for the United States (e.g., Tang et al., 2019; Allen et al., 2015) and for European countries (e.g., Madonna et al., 2018; Punge et al., 2017). Similarly, Prein and Holland (2018) examined a set of large-scale variables to estimate damaging hail frequency over the United States, while also testing the suitability of their approach at the global scale. Hail models have been constructed by using different combinations of predictors (i.e. multivariate approaches) to take into account the specific environmental conditions required for the development of a convective storm which includes aspects of thermodynamic (e.g., convective energy needed to feed and maintain strong updrafts), kinematic (e.g., vertical wind shear, to organize the convective storms) and atmospheric instability (e.g., lifting mechanisms to overcome the convective inhibition in the boundary layer (Santos and Belo-Pereira, 2019)). The relative importance of these conditions also depends on regional factors, such as orography, thermo-topographic wind systems, and the presence of water bodies (Mohr et al., 2015a) which lead to spatial heterogeneity in the hail storm responses (Raupach et al., 2021). The methods that have been used for the construction of the hail models range from regression techniques, such as partial least square regression and principal component regression (Eccel et al., 2012), logistic or Poisson models (Madonna et al., 2018) random forest (Czernecki et al., 2019), and neural networks (Manzato, 2013; Marzban and Witt, 2001), among others.

The main goal of this work is the development of a model that provides hail probability over Italy in the 1979–2020 period. The model is based on the multivariate methodology described in Prein and Holland (2018), but with several modifications to better describe the hail conditions in the Italian domain. We have considered the ERA5 large-scale environmental variables (Hersbach et al., 2020) as potential predictors of hail-favourable conditions from the European Severe Weather Database (Groenemeijer et al., 2017). We have extended the Prein and Holland (2018) methodology by using a genetic algorithm to identify objectively the optimal set of predictors. Moreover, two independent models have been produced: a General Hail Model (GHM) and a Severe Hail Model (SHM), which differ by the subset of hail observations used for the model calibration. These models provide homogeneously-spaced information at daily frequency, thus offering a suitable framework to characterize the variability of the hail hazard over Italy. The validation has been performed against an independent observational data source

over Friuli Venezia Giulia which is a small region located in northeast Italy (see Figure S1 in the supplementary material).

The manuscript has been organized as follows: Section 2 describes the employed datasets, Section 3 details the hail model, and Section 4 presents the main results of the paper. The results include the hail observations over Italy (Section 4.1), the influence of large-scale variables and convective indices on the hail development (Section 4.2), the description of the hail probability obtained from the model (Section 4.3), and the validation of the model over the Friuli Venezia Giulia region (Section 4.4). Section 5 includes a discussion of the main outcomes of this work. Finally, the main conclusions are described in Section 6.

2. Data description

2.1. European severe weather database (ESWD) hail data

The European severe weather database (ESWD, <https://www.eswd.eu/>) collects and provides detailed and quality-controlled information on severe convective storm events over Europe. This database is maintained by the European Severe Storms Laboratory (ESSL), but it relies heavily on voluntary observers networks, weather enthusiasts, news and media and national hydro-meteorological services. Therefore, the majority of the ESWD hail reports are collected in densely populated areas. Due to the high interest of the public in extreme meteorological events and technological improvements, the number of volunteers contributing to the ESWD has increased in the latest years. These volunteers report hail observations that are checked with a step-by-step quality-control system (Groenemeijer et al., 2017; Dotzek et al., 2009). Nevertheless, these reports might be affected by spatial inhomogeneity, as they are intrinsically biased towards large hail and densely populated areas, where hail events are more important and population awareness is high. Moreover, hail size information is often affected by large uncertainties because of subjective estimations and/or indirect measurements (Punge and Kunz, 2016; Allen et al., 2015). The type of severe weather events included in ESWD are avalanches, tornadoes, gust front vortex, lesser whirlwinds, lightning, ice accumulation, snow, severe wind gust, and hail. Particularly, ESWD is the most extensive archive for hail reports in Europe and it contains information about the date, hour, hail size, and location of the hail event. In this work, we have considered ESWD hail data over the Italian domain [6–19°E, 36–48°N] for the 2000–2020 period. A total of 2074 reports were available, of which 1159 include information on the hail diameter (Fig. 1a). The whole set of observations is employed for the construction of the GHM whereas a subset of 729 observations (those with hailstones diameter greater than 2.5 cm) is employed for the SHM. The ESWD hail observations for the 2021 and 2022 hail seasons were not included in the training set, as they were not available at the time of preparing this manuscript. Hence, they have been considered as an independent dataset from the training data, and they have been used to assess the performance of the hail models over the full Italian domain in these two years (see supplementary material, Section S1).

2.2. ARPA Friuli Venezia Giulia hail data

The Agenzia Regionale Per l'Ambiente (ARPA) Friuli Venezia Giulia hail database (ARPA FVG, <https://www.meteo.fvg.it/grandine.php>) is a regional dataset of hail events, based on a network of hail pads located in the plain areas of the Friuli Venezia Giulia region, at the northeastern margin of Italy (Fig. 2). This dataset has been made available recently, but the network was established in 1988 and it is still operative, despite the degree of involvement of some volunteers may have decreased over time. The database considered for this study covers the hail season (April to September) during the period 1988–2016 and includes around 6600 individual pads, distributed over 240 locations (Fig. 2a).

The collection of hail data for the ARPA FVG database is not straightforward as it implies human control of the pads right after

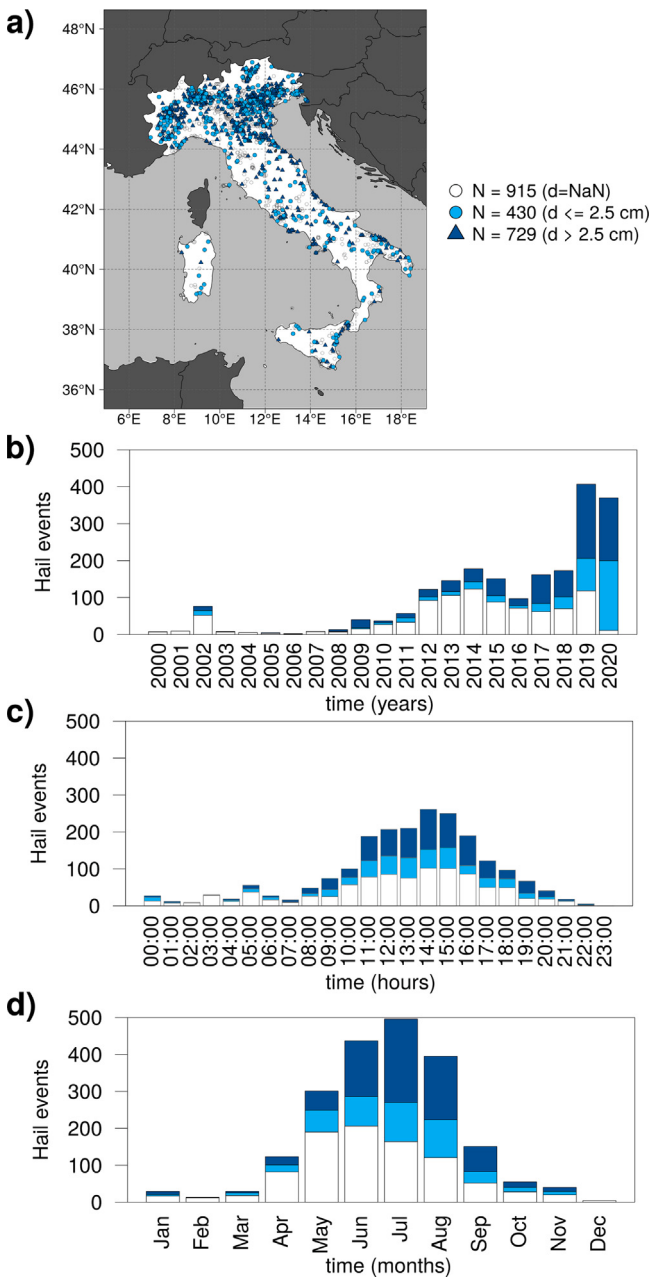


Fig. 1. (a) European Severe Weather Database (ESWD) hail events over the Italian region in the 2000–2020 period. (b) Year-to-year distribution of the ESWD hail events aggregated over Italy (c) Number of ESWD hail events per hour (UTC) of the day (d) Number of ESWD hail events per month. The hail events have been classified into three different categories: hail events without diameter information (white), hail diameter less than or equal to 2.5 cm (light blue) and hail diameter larger than 2.5 cm (blue). (For interpretation of the references to colour in this figure legend, the reader is referred to the web version of this article.)

the event. Most of this work is carried out by volunteers, whose number, availability and experience have fluctuated over the years. These issues might lead to a potential underestimation of the number of events, for example when two or more hail episodes occurred without pad replacement. Another potential human-induced error comes from incorrect temporal assignments. For the measurement of hail diameter and hits density over the pads, a semi-automatic analysis is pursued by the software TITAN (Manzato et al., 2020; Dixon and Wiener, 1993). Still, the pad itself can be damaged or deformed by handling, birds, falling objects and other independent circumstances. Nevertheless, the

ARPA FVG observations have been used in a variety of studies in the region (e.g., Manzato, 2012; Giaiotti et al., 2003, 2001).

The ARPA FVG database is a trade-off between the high time and space resolution of the hail pads based hail reports, and the need for sufficient reliability of the hail information which is achieved by aggregating the data. Therefore, observations are aggregated in time (daily — from 00 UTC to 24 UTC) and space (four domains, approximately 30×45 km large). The four domains are equally represented throughout the time series and they account, on average, for the same number of stations (Fig. 2b). Each hail event corresponds to a specific hail report on each day and domain and it includes the date, number of hit pads in the domains, median and maximum diameter, density of hits and kinetic energy flux.

2.3. ERA5 data

The ERA5 reanalysis has been used for the characterization of the large-scale atmospheric conditions leading to hail events. ERA5 is the latest European Centre for Medium-Range Weather Forecast (ECMWF) atmospheric reanalysis (Hersbach et al., 2020), based on a version of the ECMWF atmospheric model (Integrated Forecasting System, cycle 41r2) operational in 2016, which employs a four-dimensional variational analysis (4D-Var) for data assimilation. This reanalysis is particularly useful to characterize the large-scale atmospheric conditions leading to hail events at the local scale because it has a spatial resolution of approximately 30 km, 137 vertical levels and a time resolution of 1 h. In this study, we used ERA5 data in the 1979–2020 period.

The ERA5 variables considered in this work are listed in Table 1. Some of these variables have been directly extracted from the reanalysis (at surface and pressure levels), while others (storm-relative helicity, wind shear and the temperature and relative humidity gradients) have been derived from ERA5 output variables. Particularly, the storm-relative helicity has been computed by using two different formulations (Prein and Holland, 2018; Bunkers et al., 2000). The choice of the initial set of potential hail predictors is primarily inspired by the different options that have been tested in the literature (e.g., Czernecki et al., 2019; Prein and Holland, 2018; Eccel et al., 2012). These sets typically include essential climate variables, convective indices and variables that are linked to the vertical structure of the atmosphere (Allen et al., 2015; Brooks et al., 2003). In addition, the joint distribution between Convective Available Potential Energy (CAPE) and Freezing Level Height (FLH) has been included, for consistency with Prein and Holland (2018). Even though the evaluation of all the different combinations between the potential predictors might be relevant, it has not been tested as the complexity of the hail model would increase enormously, just as the computational resources needed. Therefore, the final decision on the potential predictors remains, to a certain extent, subjective.

3. Methodology

3.1. Hail model

In this work, we followed the multivariate approach described in Prein and Holland (2018) to simulate the daily Probability of Hail (PH) and we applied it in the Italian domain during the April to October season. This method relies on a set of atmospheric variables and convective indices which are employed as predictors for the construction of a statistical model. The Prein and Holland (2018) methodology has been selected due to its flexibility. It does not assume any specific distribution of the predictors or any relationship between the variables, and it does not require weighting or normalization. The main steps of this methodology have been summarized in Fig. 3.

In this study, we have developed two different models: a General Hail Model (GHM) and a Severe Hail Model (SHM). The former uses all

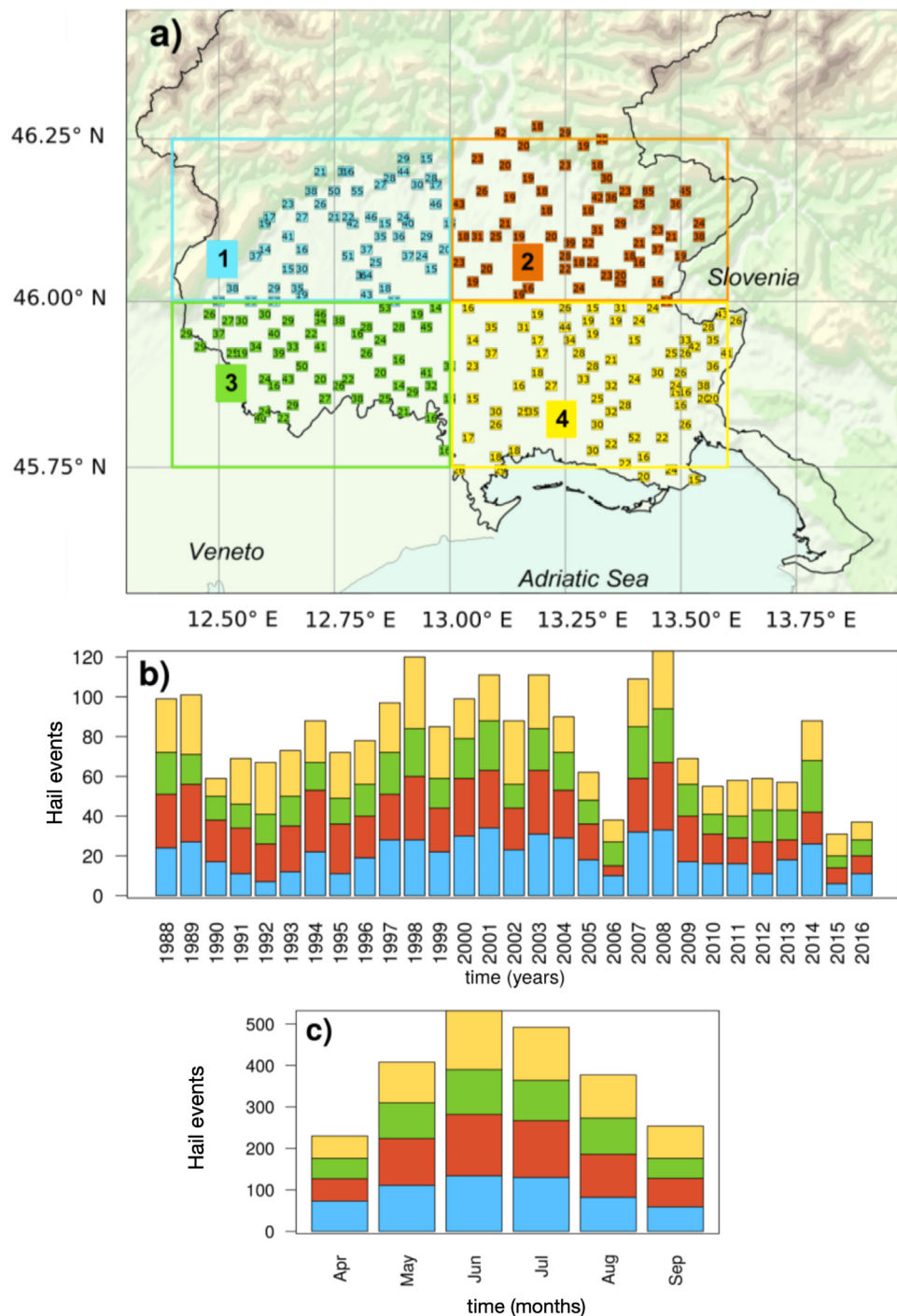


Fig. 2. (a) Location of the 240 ARPA Friuli Venezia Giulia (ARPA FVG) stations used for the ARPA Friuli Venezia Giulia hail dataset aggregated in four domains (1-blue, 2-orange, 3-green and 4-yellow). (b) Year-to-year distribution of the ARPA FVG hail events aggregated over each domain over the 1988 to 2016 period. (c) Number of ARPA FVG hail events per month.

(For interpretation of the references to colour in this figure legend, the reader is referred to the web version of this article.)

the available ESWD observations for the computation of the probability distributions conditioned on hail days. The latter considers a subset of these observations whose hailstone maximum diameter is above 2.5 cm, and therefore this model is expected to provide the probability of having environmental conditions favourable to severe hail.

We have selected a set of 18 potential predictors from the ERA5 reanalysis (Table 1). All the ERA5 variables are available at the hourly temporal resolution, but a daily value is selected at the time step the Convective Available Potential Energy (CAPE) is maximum. This choice is justified because the maximum CAPE is strongly related to the high instability needed for the hailstorm formation (Prein and Holland,

2018). Furthermore, we assumed that the moment of maximum CAPE is representative of the typical conditions for hail formation in the other atmospheric variables and the convective indices. The implications of this choice are discussed in the supplementary material (see section S3 and Figure S3). The ERA5 predictors have been selected in the nearest grid point to the location of the hail observation. In addition, a region of ± 2 grid points around the hail observation has been considered to account for the potential spatial mismatch between the actual hail environment and the reanalysis fields (Prein and Holland, 2018). Therefore, nine grid points are employed for the construction of the conditioned probability distribution of each ERA5 variable.

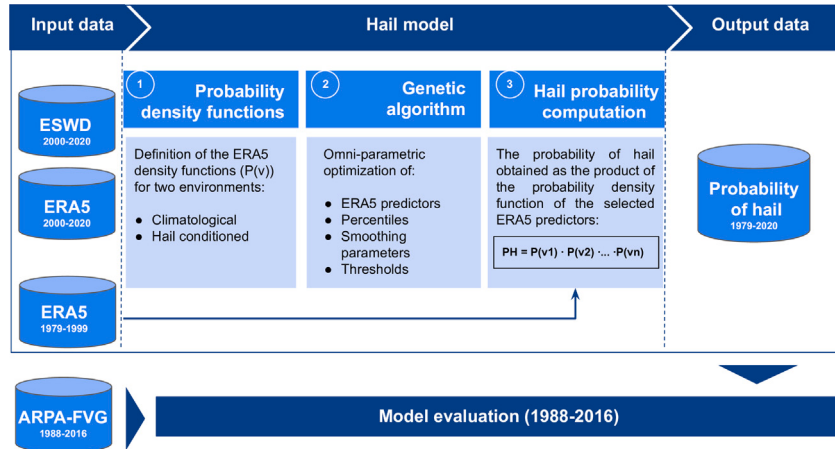


Fig. 3. Workflow to summarize the main steps followed for the implementation of the hail model. The model has been calibrated with the ESWD hail observations and the ERA5 variables in the 2000–2020 period. The method generates the hail probability dataset at daily resolution for the extended hail season (April to October) from 1979 to 2020. The performance of the hail model has been assessed by comparing the probability of hail with the observational ARPA FVG dataset.

Table 1

ERA5 variables considered in this study. They have been used in the 1979–2020 period with hourly resolution. The superscripts in the acronyms indicate if that specific variable has been selected as a predictor for the generalized (G) hail model and for the severe (S) hail model. These predictors are described in the supplementary material (Section S2).

Acronym	Variable	Unit
BLH ^G	Boundary layer height	m
CAPE ^{G,S}	Convective available potential energy	J kg ⁻¹
CBH ^{G,S}	Cloud base height	m
CIN ^S	Convective inhibition	J kg ⁻¹
FLH ^{G,S}	Freezing level height	m
KI ^S	K-Index	K
RH500–700	Relative humidity gradient (500–700 hPa)	m ⁻¹
T500–700	Temperature gradient (500–700 hPa)	K m ⁻¹
Td2M	2 m dew point temperature	K
T2M	2 m temperature	K
TCWV	Total column water vapour	kg m ⁻¹
TOTALI ^{G,S}	Total totals index	K
SSHF	Instantaneous surface sensible heat flux	W m ⁻¹
SRHBU	Storm relative helicity Bunkers ^a	m ² s ⁻²
SRHPR	Storm relative helicity Prein ^a	m ² s ⁻²
VIDMF ^G	Vertical integral of divergence of moisture flux	kg m ² s ⁻¹
WSH3 ^S	Bulk wind shear 0–3 km ^a	m s ⁻¹
WSH6 ^G	Bulk wind shear 0–6 km ^a	m s ⁻¹

^aThe variables have been derived from ERA5 output variables.

The conditioned probability distributions (P_{v_i}) of each predictor v_i are defined as in Prein and Holland (2018). We have used a hyperbolic function that is meant to cover the range of values associated with hail-favourable environmental conditions, compared to the climatology (step 1 in Fig. 3). The equation of the function reads:

$$P(v_i) = \begin{cases} 0.5 + 0.5 \cdot \tanh\left(\frac{x - \frac{x_{p_1} + x_{p_2}}{2}}{(x_{p_1} - x_{p_2}) \cdot c}\right) & x < \frac{x_{p_2} + x_{p_3}}{2} \\ 1 - \left[0.5 + 0.5 \cdot \tanh\left(\frac{x - \frac{x_{p_3} + x_{p_4}}{2}}{(x_{p_4} - x_{p_3}) \cdot c}\right)\right] & x \geq \frac{x_{p_2} + x_{p_3}}{2} \end{cases} \quad (1)$$

where x_{p_1} , x_{p_2} , x_{p_3} , x_{p_4} are the actual values assumed by the predictor (x), corresponding to the p_i th percentile and c is a smoothing parameter, a positive constant controlling the smoothness of the transition between hail-favourable and non-favourable environment, that is the smoothness of the ascending and descending branches of the function.

The percentiles can be directly obtained from these equations:

$$\begin{cases} p_1 = p_{tail} \\ \Delta p = p_2 - p_1 \\ p_4 = 100 - p_1 \\ p_3 = p_4 - \Delta p \end{cases} \quad (2)$$

p_{tail} and Δp are parameters employed for the truncation of the hail environments. p_{tail} is employed to truncate the hail environmental probability density function equally on both sides, Δp is used to achieve the same smoothness of transition from hail to non-hail environments on both tails of the distribution. Hence, the definition of the probability functions for each predictor eventually depends on three parameters only: Δp , p_{tail} , and the coefficient of smoothing c . Prein and Holland (2018) obtained these parameters through optimization metrics, whereas in this work the optimization is performed by a Genetic Algorithm (GA, step 2 in Fig. 3) which allows us to generalize the optimization process.

The PH is computed as the product of the probability distributions of the selected predictors as follows (step 3 in Fig. 3):

$$PH = P_{v_1} \cdot P_{v_2} \cdot \dots \cdot P_{v_n} \quad (3)$$

An additional parameter is provided by the GA optimization (p_t) to convert the final PH (Eq. (3)) into a binary field describing the hail occurrence. The p_t parameter consists of a threshold for the PH, and it is used as follows:

$$hailday = \begin{cases} 1 & PH \geq p_t \\ 0 & PH < p_t \end{cases} \quad (4)$$

3.2. Genetic algorithm

The Genetic Algorithm (GA) is a method based on the translation of Darwin's assessment of the natural selection of organisms to machine learning areas (e.g., Haupt and Haupt, 2004; Mitchell, 1998; Goldberg and Holland, 1988). This methodology has shown strong potential for the hail model development. The GA has been applied to obtain the Δp , p_{tail} and the coefficient of smoothing, as well as for objectively identifying the best set of predictors among the 18 ERA5 indicators considered. In this regard, the GA optimized a total of 162 parameters (18 ERA5 potential predictors and the 9 grid points around the hail event).

The input data of the GA include both the hail events and the non-hail events, derived from the ESWD observations, together with the

corresponding ERA5 variables. At first, hail observations are aggregated on the ERA5 grid, which means that if several reports refer to the same event, they have been counted only once. For the GHM (SHM), 2074 (729) available reports have resulted in 1250 (474) hail events in the 2000–2020 period. Hail events and non-hail events represent, respectively, the minority and majority classes of a canonical imbalanced data learning process. The minority class is typically the class of interest, as it is for the occurrence of an extreme event, but learning algorithms tend to be biased towards the majority class (that is, over-predicting), whose occurrences are more frequent. The disproportion between classes is a well-known issue in machine learning and it has been addressed with different approaches (see Fernández et al., 2018 for a review). In this work, a non-hail event at a specific location is defined by the absence of hail reports and convective precipitation. Therefore, the majority class (non-hail events) has been populated with two different sets: (1) non-hail events that occur on the same day of a hail event but in different locations (and with convective precipitation equal to zero) and (2) non-hail events that occur in the non-hail days and which show convective precipitation equal to zero. Then, the random selection across these subsets is obtained by ensuring the representation of non-hail days in each month (i.e. stratification by month). Each set counts twice the number of hail events in the respective model so that the imbalance ratio is set to 1/4. This value is in agreement with similar problems, even though comprehensive studies on extremely imbalanced datasets are still lacking (Krawczyk, 2016). Hence, the GA processes 6250 (2370) events for the GHM (SHM) of which 1250 (474) are hail events and 5000 (1896) are non-hail events.

The workflow for the application of a GA can be summarized in three main steps (Katoch et al., 2021): selection, evolution and fitness function computation. The first step is the selection of a random population. In the evolution phase, the algorithm derives a second-generation population of solutions from the initial population by employing two genetic operators: crossover and mutation. The crossover is controlled by the crossover probability, which quantifies the chances that two individuals can exchange some of their parts (1 indicates that all offspring are made by crossover and 0 indicates if the new generation is a copy of the older population). The crossover probability is 0.5 (Table 2). To guarantee diversity in the population and avoid premature convergence, the mutation stage is applied to the new offspring that will be added to the population. The mutation is controlled by the mutation probability that ranges from 0 to 1, and in this work, it is set to 0.15. In the last step, the resulting new population is assessed by the GA fitness score (Eq. (5)). The individuals with the best GA fitness score (elite) are retained for the next generations. In this work, 10% of the individuals have been retained as elite solutions (Table 2). This process is applied over a certain number of iterations to obtain the population with the minimum GA fitness score value and the optimal solution. These parameters have been selected according to the recommendations of previous works (e.g., Hassanat et al., 2019). The maximum number of iterations employed in this work is 175 and the population size is 150 (Table 2). The GA parameters used for the construction of the SHM are in the supplementary material (Table S1). Among the GA parameters, the number of iterations and the initial population size are the most critical ones (Mills et al., 2015) and therefore sensitivity tests have been performed to quantify their effect on the GA fitness score. We have applied these sensitivity tests for the samples corresponding to the GHM and the SHM separately and iteration values between 125 and 225 and population sizes between 25 and 150 have been considered. Each test has been replicated 20 times, to obtain robust estimates of the GA optimization scores. The range of values for the parameters has also been selected by taking into account the computational costs and the added value of increasing both the number of iterations and population size.

To evaluate the fitness of each member of the population we have employed a fitness function defined as:

$$J = 1 - MCC \quad (5)$$

Table 2

Genetic algorithm parameters for the general hail model.

Number of iterations	175
Initial population size	150
Mutation probability	0.15
Crossover probability	0.5
Elite percentage	10%

Table 3

Selected variables and corresponding parameters for the general hail model ($p_c = 0.0049$). CAPE-FLH is the bivariate predictor resulting from the joint probability of CAPE and FLH. Note these variables are listed in alphabetical order as the GA does not provide ranked predictors.

	p_{tail}	Δp	c
BLH	1.9	25	0.31
CAPE	0.99	13	0.3
CAPE-FLH	3.02	19	0.26
CBH	5.89	7	0.32
TOTALI	3.5	5	0.31
VIDMF	1.12	29	0.32
WSH6	1.25	8	0.27

where J is the GA fitness score and depends on the Matthews Correlation Coefficient (MCC):

$$MCC = \frac{a \cdot d - b \cdot c}{\sqrt{(a+b)(a+c)(d+b)(d+c)}} \quad (6)$$

MCC (Boughorbel et al., 2017) considers the results of the contingency table: true positive/hits (a), false positive/false alarm (b), false negative/misses (c) and true negative/correct negative (d). The GA score depending on the MCC coefficient is particularly useful for this work as it provides balanced model accuracy assessment for imbalanced datasets (i.e. different proportions of positive and negative occurrences of hail) (Chicco and Jurman, 2020) and it guarantees the optimal subset out of the 162 parameters. Furthermore, the MCC might be more useful than some other potential fitness functions (Chicco et al., 2021). MCC varies in [-1,1] where -1 indicates a perfect disagreement between the actual value and the estimation and 1 indicates a perfect agreement.

The output of the GA optimization has been included in Table 3 for the GHM and in Table S2 included in the supplementary material for the SHM. The output of the GA optimization consists of the best set of predictors from the initial list of ERA5 potential candidates (Table 1). In addition, the GA also provides the parameters needed for the construction of the probability distributions of these selected predictors (Fig. 4). The GA does not provide a ranking of predictors. The GA solution corresponds to those combinations of variables and parameters which minimize the GA score (Eq. (5)).

3.3. Model evaluation metrics

The performance of the general hail model has been evaluated in a region in northeastern Italy by using the ARPA FVG observational dataset as a reference. For the assessment of the GHM, all the ARPA FVG hail observations have been used whereas the performance of the SHM has been evaluated by using the ARPA FVG hail observations whose diameter exceeds 1.25 cm (see Figure S2). This diameter has been selected because the maximum hail diameter provided by the hail pads is usually half the size of the maximum hailstone observed in the vicinity (i.e. 2.5cm), as it is discussed in Manzato et al. (2022a) and references therein. For the assessment of the hail models, we have employed several metrics. Pearson's correlation coefficient (Wilks, 2011) has been used to measure the agreement between the monthly mean PH and the total number of observed occurrences per month. This metric allows us to quantify the ability of the model to represent the inter-annual variability of the hail events. The statistical significance of these correlations has been determined by a t-test with a 95% confidence level.

The evaluation of the binary hail events has been carried out by employing different performance measures based on a 2×2 contingency table (Jolliffe and Stephenson, 2012 and references therein). The equations related to the categorical metrics have been included in the supplementary material (Table S3). For this categorical analysis, the maximum probability of hail in the target domain has been transformed into hail occurrences by employing the probability threshold given by the GA optimization (i.e. a hail day is considered when $\text{PH} > p_t$ and $p_t = 0.0049$, as included in Table 3). Then, the contingency table has been used to compute the probability of detection (POD) which measures the accuracy of the hail model to identify hail days. POD varies from 0 to 1, and $\text{POD} = 1$ indicates a perfect estimation of the hail days. The POD can be complemented with the Miss rate (MR) which measures the fraction of hail days that were not correctly detected. The False Alarm Ratio (FAR) quantifies which fraction of the estimated hail days actually did not occur, therefore $\text{FAR} = 0$ refers to a perfect model. The Peirce Skill Score (PSS, Peirce, 1884) has been used to explore if the hail model correctly differentiates between "hail" and "non-hail" days, and it is particularly useful for rare events such as hail (1250 events in the 2000–2020 period). PSS = 1 indicates the hail model perfectly discriminates situations that lead to the occurrence of the event from those that do not and PSS = 0 shows the hail model is not able to discern "hail" from "non-hail" days.

4. Results

4.1. Hail observations over Italy

The spatial distribution of the ESWD hail data is mostly concentrated in northern Italy and coastal regions (Fig. 1a). These regions have valuable infrastructures and agricultural activities (Baldi et al., 2014), which make them extremely vulnerable to the hail hazard. Fig. 1b shows the number of ESWD events registered in the 2000–2020 period. The increase in the number of records for the latest years is more likely the consequence of a higher engagement of volunteers in reporting these events than a hail frequency trend (Groenemeijer et al., 2017). The increase in registered hail events started in 2009, but some exceptions are also found. For example, in 2002, more than 24 hail events were reported. Nevertheless, it is important to mention that more than 50% of the hail events used here are concentrated only in 2019 and 2020. Regarding the severity, year-to-year fluctuations are also observed. For example, in 2009, 18 out of 25 events showed hail diameters larger than 2.5 cm. The number of hail observations for the ARPA FVG region is homogeneously distributed during the 1988 to 2016 period with the maximum number of records in 1998 and 2008 and the minimum in 2006, 2015, and 2016 (Fig. 2).

ESWD observations for Italy show that hail mostly occurs in the afternoon (Fig. 1c), similarly to other European Countries (Fluck et al., 2021; Nisi et al., 2016). Nevertheless, hail events are identified for all hourly intervals. Particularly, the maximum is obtained from 14:00 to 15:00 UTC which is related to the daily cycle of convection, near-surface temperature and the resulting increase of potential temperature lapse rate (Punge and Kunz, 2016).

Most events in Italy occur between April and October (Fig. 1d), being June and July the months with the highest frequency (~40% of the hail events occur in these two months). A similar pattern of variability has been observed in other European neighbouring countries, through a variety of data sources (e.g., Jelić et al., 2020; Kunz et al., 2020; Púčik et al., 2019). The hail activity is mostly concentrated in these months due to the warm temperatures that increase atmospheric instability. These results are also consistent with the distribution of hail reports in ARPA FVG data (Manzato et al., 2022b; Gaiotti et al., 2003), with the peak month in June, followed by July and May (Fig. 2c).

4.2. Environmental conditions for hail events over Italy

To understand the ability of the GA-selected predictors to differentiate between hail and non-hail environments, we analyse the relationship between the ERA5 predictors and the probability of having hail over the Italian domain, on a daily basis. This analysis has been performed for both GHM and the SHM (Fig. 4). The corresponding results for the joint distribution of CAPE and FLH are included in the supplementary material (Figure S4). These probability distributions have been constructed from the percentiles estimated with the genetic algorithm (Table 3 and Table S2) and with the equations detailed in Section 3.1.

CAPE distributions are different when suitable conditions for hail are present or not, as shown by the separation between the red and black lines (Fig. 4a). All variables have similar behaviour, with the only exceptions of the BLH and VIDMF (Fig. 4d and e, respectively), whose peak values are nearly identical in both hail and climatological environments. When CAPE values are above 500 J/kg (solid blue curve in Fig. 4a), the atmospheric conditions are generally favourable to hail. Then, high CAPE values (around 1000 J/kg) are needed for environmental conditions to be suitable for a severe hailstorm (Fig. 4a, dashed line).

The KI and TOTALI indices show variations between 20–40K and 45–60K, respectively, for potential hail occurrences. CBH values show similar values for severe and non-severe events (Fig. 4b dashed and solid blue lines, respectively), with values ranging between 200 and 3200 m for both cases. CIN values ranging between 0 and 400 (Fig. 4g) are indicators of days inclined to develop hail events, with the highest probability for CIN values around 200 J/kg. Indeed, CIN may contribute to establishing a build-up of energy that maximizes CAPE resulting in stronger convection (Taszarek et al., 2020). Similarly, WSH3 values between 10 and 25 m/s (Fig. 4i) and WSH6 values between 5 and 40 m/s (Fig. 4f) suggest strong potential for hailstorm development.

Fig. 4d shows a variety of BLH values suitable for the establishment of hail conditions. However, most events in this work are associated with $BLH \approx 200$ m, close to the climatological value.

4.3. Characterization of the hail probability over Italy

As described in the previous section, the GA provides all the elements needed to define the daily probability of hail (PH), obtained as a simple product of the individual probabilities of the selected variables. For the GHM this can be obtained as follows:

$$PH_{GHM} = P_{CAPE} \cdot P_{CAPE,FLH} \cdot P_{CBH} \cdot P_{TOTALI} \cdot P_{BLH} \cdot P_{VIDMF} \cdot P_{WSH6} \quad (7)$$

For the SHM the hail probability has been computed as:

$$PH_{SHM} = P_{CAPE} \cdot P_{CAPE,FLH} \cdot P_{CBH} \cdot P_{TOTALI} \cdot P_{CIN} \cdot P_{KI} \cdot P_{WSH3} \quad (8)$$

Hence, PH is, by definition, a quantity that varies in [0,1]. PH equals one when each of the individual predictors assumes, on that day, probabilities equal to one, which is statistically associated with hail-favourable conditions (Fig. 4). However, being PH the product of a number of predictors' probabilities, PH is generally much lower than one (Figure S5 in the supplementary material).

Being the PH index probabilistic, an additional choice is required to relate its outcome to observations: what is the threshold the PH should exceed, to consider that day a potential hail day? While this type of value has been often calculated through Bayesian a-posteriori estimations (e.g., Materia et al., 2020; Nisi et al., 2016), in this case, the GA directly provides a threshold (see Table 3 and Table S2). Then, the average number of occurrences has been estimated for the hail season (from April to October, Fig. 5) and for every single month (Figs. 6 and 7) over the 1979–2020 period.

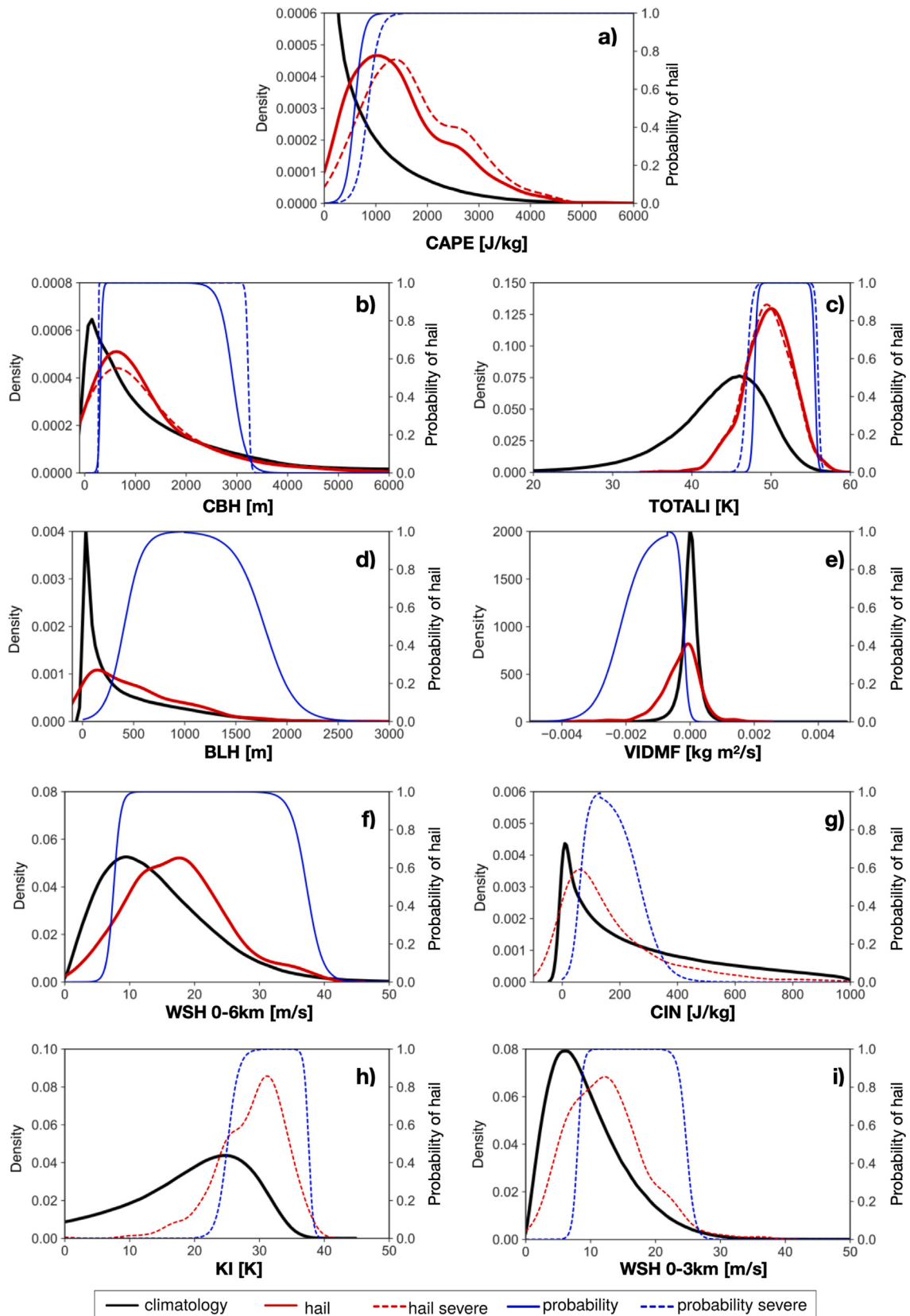


Fig. 4. Probability density functions of the (a) Convective available potential energy (CAPE), (b) Cloud base height (CBH), (c) Total of totals index (TOTALI), (d) Boundary level height (BLH), (e) Vertical integral of divergence moisture flux (VIDMF), (f) WSH between 0 and 6 km (WSH6) (g) Convective inhibition (CIN), (h) K-index (KI), and (i) Bulk wind shear between 0 and 3 km (WSH3). The black line corresponds to the climatological distribution and the red line to the hail-conditioned probability. The hyperbolic function describing the modelled probability obtained from the GA algorithm is represented as a blue line (solid — GHM, dashed — SHM). These plots correspond to the aggregated data over Italy in 2000–2020 (from April to September) period for the variables selected by the GA for the generation of the GHM and SHM. (For interpretation of the references to colour in this figure legend, the reader is referred to the web version of this article.)

Overall, the largest PH and related hail frequency (exceeding 20 events per year) are observed in the plains of northern Italy. Three main spots can be distinguished: the Venetian lowlands and lower Po valley, Lombardy's Alpine foothills, and the Piedmont plain. According to both GHM and SHM models, hail hazard is quite low in the Alps, with only a small signal on the Trentino-Alto Adige (TAA) region for the GHM. This signal corresponds to around five events per year and it is detectable along the Adige Valley (46°N - 11°E).

In Central Italy, hail frequency is high along the Adriatic coast and neighbouring inland areas (up to 15 events per year). Frequency is slightly lower along the Tyrrhenian coast where its spatial distribution is more irregular, with very localized peaks on the coast, especially in the GHM (Fig. 5a). Indeed, the annual frequency of hail events differs by up to four days between the GHM and SHM models with the most significant differences affecting Central Italy (Fig. 5c). In the South of Italy, the most hail-prone areas include the Apulia region (particularly, in the SHM, Fig. 5b) and the easternmost corner of Sicily, where frequency reaches ten events per year. As for the Alps, hail frequency is low along the Apennine mountains in both models. This specific spatial pattern related to the mountains is further investigated in the Discussion section.

The monthly variability of hail days is quite pronounced in both models (GHM — Fig. 6 and SHM-Figure S6). The GHM-SHM differences are shown in Fig. 7 to facilitate the comparison. While only a few days in April are characterized by hail-favourable conditions in the GHM (no events in the SHM), hail frequency increases in May, especially in Northeast Italy, and reaches its highest values in June, when high hazard is detected also in the northern and central Adriatic coast. In July, a few potential events are still observed by the GHM along the Alpine foothills, whereas the frequency slightly decreases in August. In September and October, the hail frequency patterns change, with an abrupt decrease of potential events in the North of Italy and a sharp increase in the South.

The PH-derived hail hazard signal in Southern Italy is mainly confined to the coastal areas, where warm temperatures persist beyond the summer months due to the sea thermal capacity, promoting atmospheric instability (Khodayar et al., 2016). In addition, in the southern Mediterranean basin, the hydrological cycle and the cyclones' activity are at their minimum during the summer, and convection is unlikely to occur (Lionello et al., 2016; Kelley et al., 2012), thus postponing the hail season with respect to northern latitudes.

The GHM provides higher hail frequency than the SHM in April, May and October (Fig. 7). In June and September, the two models are almost equivalent as the differences are mostly not significant. The SHM shows higher frequency in July and August, mainly in the Po Valley.

4.4. Hail model assessment: the Friuli Venezia Giulia region

To assess the performance of the hail models, we have employed the ARPA FVG dataset as an independent source of hail observations. The use of an independent data source is crucial to avoid over-fitting. This subsection focuses on the GHM evaluation, but the corresponding results for the SHM can be found in the supplementary material (Figures S10 and S11). The ability of the GHM to detect the inter-annual variations in the hail occurrences has been explored for the different months (April to September) from 1988 to 2016, for every single domain, but also for the full domain (i.e. hail days in at least one of the four domains) shown in Fig. 2. This analysis focuses on June, July and August (Fig. 8) as these are the months with the highest number of hail events in the FVG region. The corresponding figures for April, May and September have been included in the supplementary material (Figures S7 and S8) for consistency, but they should be interpreted with caution due to the limited number of hail records for these months.

Fig. 8 shows the number of observed hail events and the estimated probability of hail (PH) during each year and month. The variability

of the two indicators exhibits good year-to-year agreement, especially when the full domain is considered (Fig. 8, fifth-row panels). Specific months with a good agreement between the PH and the hail observations are, for example, June 1989, July 2007, or August 1994. This result has been also quantified in terms of correlations, with positive and significant values for those months. The results are consistent also for the non-favourable hail environments: low PH values correspond to a low number of detected hail events in specific months and years (e.g., June 2000, July 2006, or August 2015). Hence, the hail model is able to simulate the inter-annual variability of the number of hail events in specific boxes and months, particularly for specific years with higher or lower than normal hail occurrences. Nevertheless, there are also some months where a high PH corresponds to a low number of events (for example in June 2012).

The month with the highest correlations is July, with positive and significant correlations for all the individual domains (up to 0.7). In June, domain 4 is the only one showing non-significant correlations. In August, the correlation values are around 0.3 in most of the domains, but these correlations are not significant. This might be due to the lower number of hail records in this month compared to June and July. Nevertheless, if the full domain is considered (and the number of records also increases), the correlation becomes higher and significant, consistently with the other summer months.

The categorical evaluation of the hail model has been performed by employing the probability of detection (POD), false alarm ratio (FAR) and Peirce Skill Score (PSS), according to the probability of hail exceeding the probability threshold (p_t) given by the GA. These metrics have been already employed in previous studies to assess the potential of the hail model to differentiate between "hail" and "non-hail" days (e.g., Nisi et al., 2016; Mohr et al., 2015a; Manzato, 2012).

Fig. 9 shows that in June, POD values are higher than for July and August. The highest POD is obtained for domain 3 in June, domain 4 in July and domain 1–4 in June. In all the individual domains, FAR is higher than the POD, which suggests that the GHM overestimates the hail occurrences. Conversely, the results for domain 1–4 show that the POD is higher than the FAR when the hail observations are aggregated, suggesting that the hail model holds discrimination (model output is different depending on the observed outcome) when the considered domain is large. The regional variations within the FVG domain have been analysed through the individual assessment of the different domains. The best PSS values are obtained for domain 3 in June and August and for domain 4 in July. The FAR values are quite high for the individual domains, but they drop below 0.5 when the full domain is considered. The specific values of the contingency table and the metrics for each case have been included in the supplementary material (Table S4).

5. Discussion

5.1. Assessment of the hail frequency derived from the PH

In this work, the hail conditions over the Italian domain based on the probability of hail have been explored. Previous studies have suggested that the area South of the Alps is the European region most prone to large hail events (e.g. Punge and Kunz, 2016; Mohr et al., 2015b). The spatial patterns of the hail climatologies presented in this work resemble the ones obtained in other studies (e.g. Prein and Holland, 2018; Baldi et al., 2014), although the absolute frequencies given by the GHM and the SHM are higher (as so it is the spatial resolution). Conversely, in Punge et al. (2014) which provided hail frequency at 0.1° , both the hot spots and the related hail frequencies agree quite well with the GHM and SHM (up to 20 events per year). These hot spots are related to several hail episodes that have been discussed in the literature as in Laviola et al. (2020) and Manzato et al. (2020) (northeastern Italy), in Montopoli et al. (2021) (Adriatic coast),

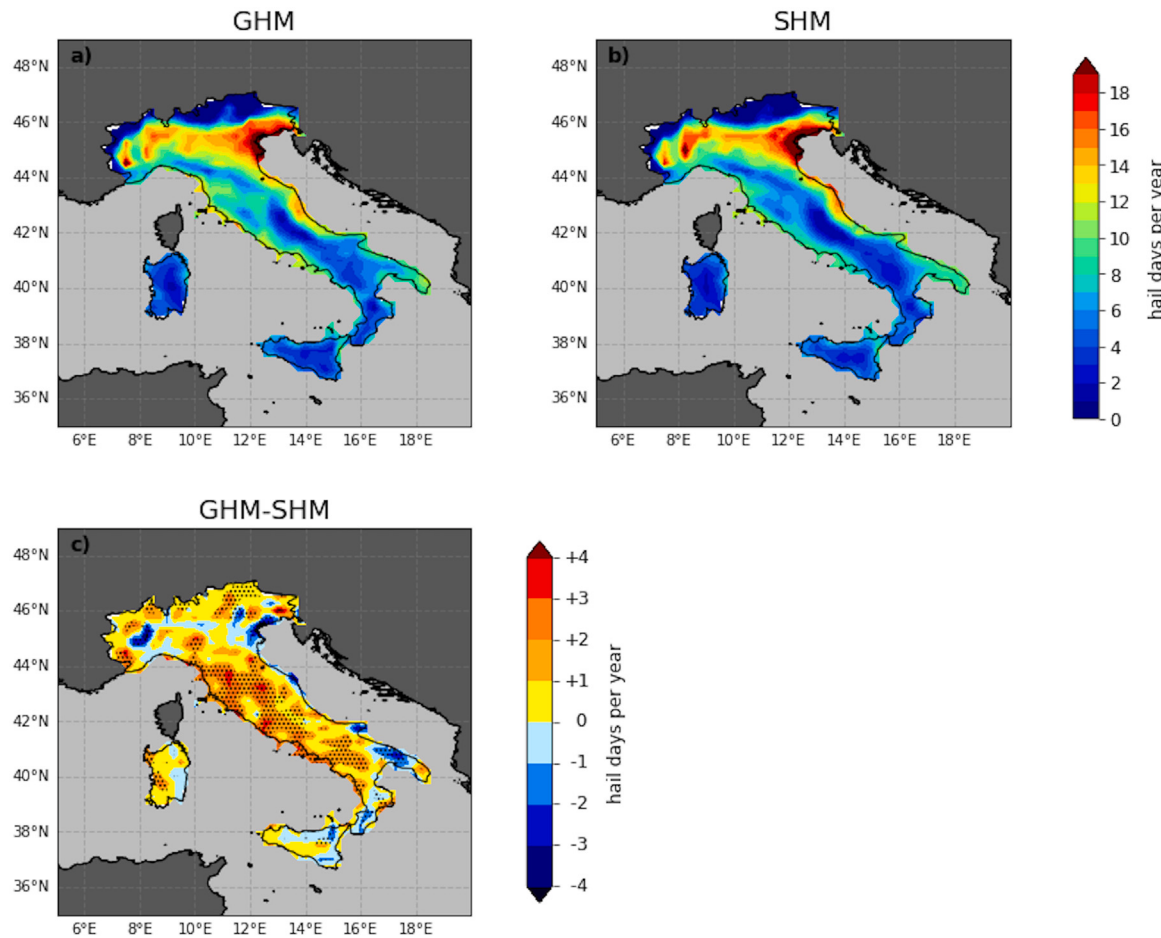


Fig. 5. Average of the estimated hail days according to the (a) GHM and (b) SHM and estimated (c) GHM-SHM hail days difference. The number of hail days corresponds to the hail season (April to October) from 1979 to 2020. Stippling indicates statistically significant differences ($p - \text{value} < 0.05$).

in Roberto et al. (2016) and Marra et al. (2017) (Tyrrhenian coast) and in Vulpiani et al. (2015) (eastern Sicily).

The results from both models show a gradient between mountain areas and neighbouring flatlands or coastal areas. Orography-induced mechanisms are known to foster convective instability. However, the number of days with favourable hail conditions over the mountains is low according to the output of our models. For example, it is known that Trentino-Alto Adige (TAA) region in the northeast of Italy is particularly inclined to hail hazard (Eccl et al., 2012). Indeed, the region is well-known for the thunderstorms and hailstorms that damage its typical apple orchards, for which mitigation and prevention tools have been largely put in place, including a widespread anti-hail nets system (Rogna et al., 2021; Baiamonte et al., 2016). Impacts on crops and fruit plants can be dramatic even with small to medium-size hailstones (Púčik et al., 2019) and this raises, even more, the vulnerability to hail events in those areas. As pointed out in Section 4.3, TAA does not stand as a hail hotspot in our models. There are two main explanations for this inconsistency. First, the complex topography in reanalysis products such as ERA5 is smoothed. Despite the higher horizontal resolution of ERA5 with respect to previous reanalyses, the complex pattern of Alpine valleys is still not fully represented (Muñoz Sabater et al., 2021). The lower model levels and the corresponding weather fields relate to a smoothed orography, thus affecting the reliability of some of the predictors as CAPE and CIN (Markowski and Dotzek, 2011) which reflects on the PH itself. Second, the number of reports in the ESWD database referring to mountain areas is generally low, due to the bias of voluntary-based hail reports towards densely populated and urban locations. Therefore, the GA might not have proper coverage of

mountain hail events to be used for the optimal selection of the weather predictors.

5.2. Comparison of GHM and SHM

As already mentioned, the GHM leads to higher hail frequency in the mountains, including TAA (Fig. 5c). It also provides slightly better results in terms of verification metrics when validated in domains 3 and 4 compared with domains 1 and 2 (Fig. 9). Domains 1 and 2 include stations at high elevations, where the hailstorms are mainly linked to orographic processes (Manzato, 2012; Giavotti et al., 2003). Even though the differences in the values of the verification metrics are quite small, they are coherent throughout the months. On the other hand, higher frequencies (up to 3 events per year) are observed in the SHM over a few well-known hotspots for damaging hail, along the Po Valley and the Adriatic coast. In terms of variability, the hail season in the SHM is shifted towards late summer with respect to the GHM. A slightly better performance of the GHM compared to the SHM can be also seen for 2021 and 2022 when the full Italian domain is considered (supplementary material, Section S1). All these differences between the two models come from (1) the different sets of events that have been used for calibration and (2) the consequent different sets of variables selected by the GA.

For example, CAPE, joint CAPE and FLH, CBH and TOTALI are shared between the two models. The wind shear is also shared but within different levels, 0–6 km for the GHM and 0–3 km for the SHM. Then, the SHM includes CIN and KI, in place of BLH and VIDMF which belong to the list of GHM predictors. The selected predictors suggest

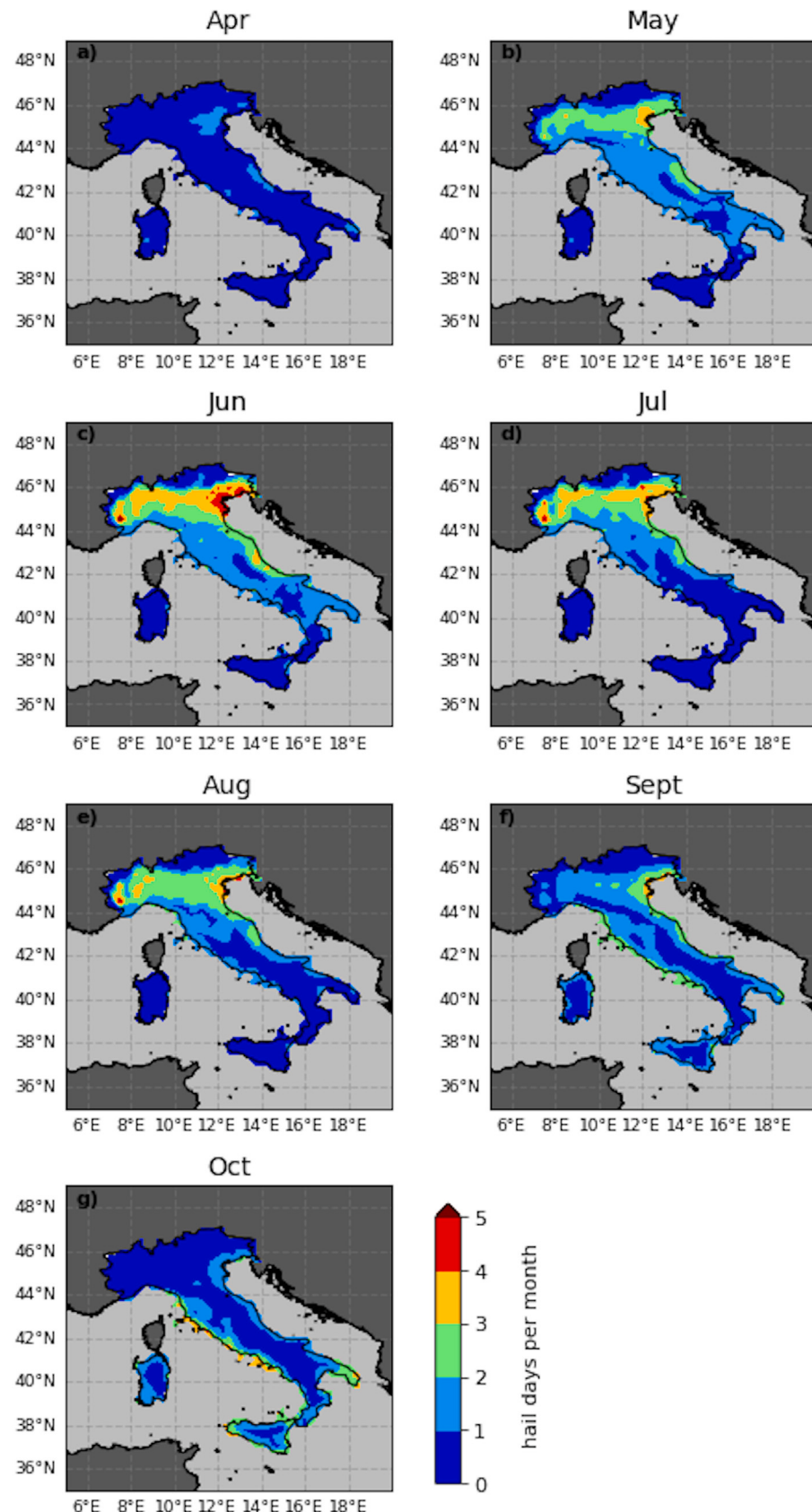


Fig. 6. Monthly average of the estimated hail days according to the GHM in 1979–2020.

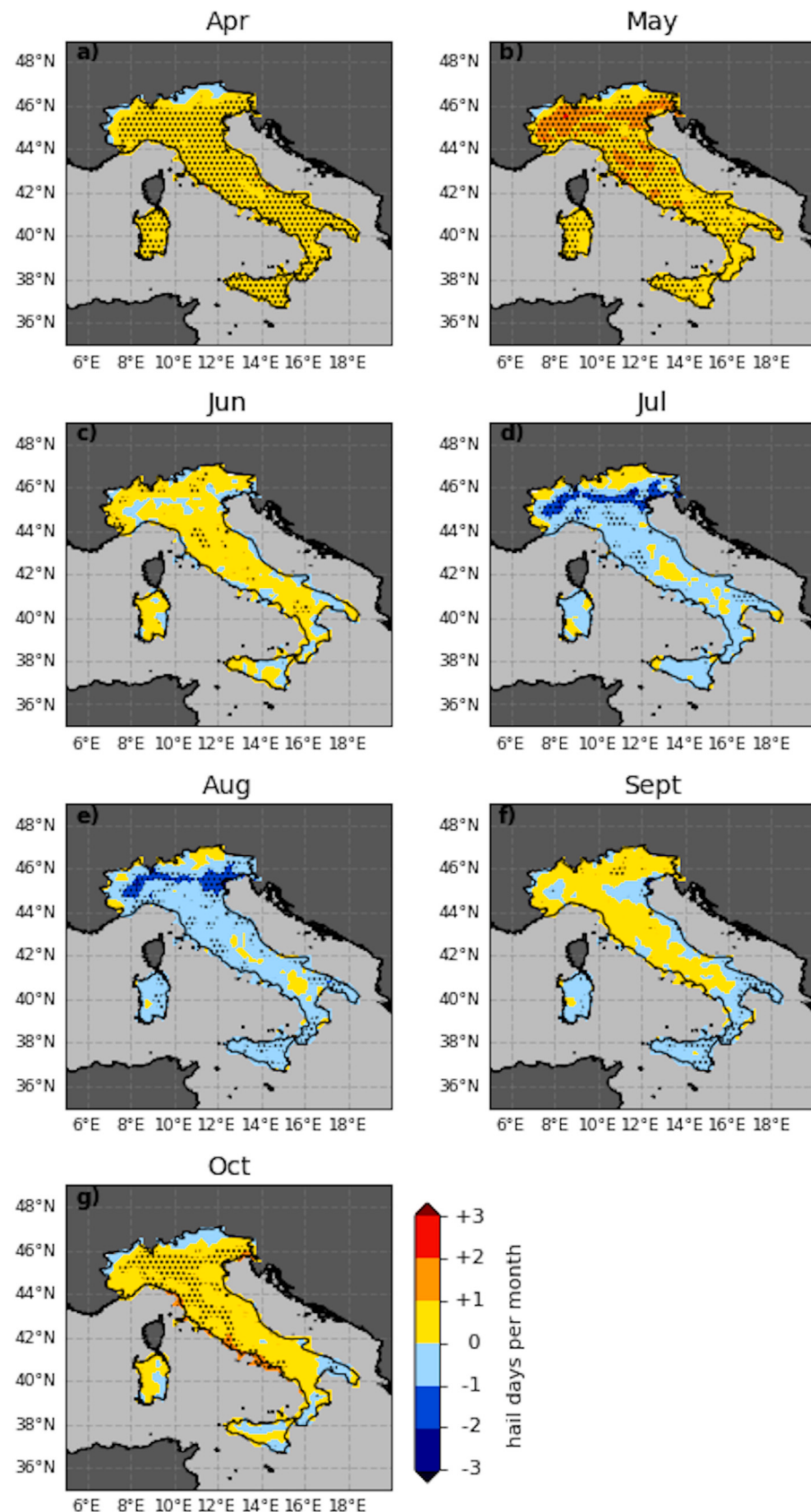


Fig. 7. GHM-SHM differences corresponding to the monthly average of the estimated hail days for 1979–2020. Red (blue) shading indicates that the number of hail days is higher (lower) in GHM than in SHM. Stippling indicates statistically significant differences (p -value < 0.05). (For interpretation of the references to colour in this figure legend, the reader is referred to the web version of this article.)

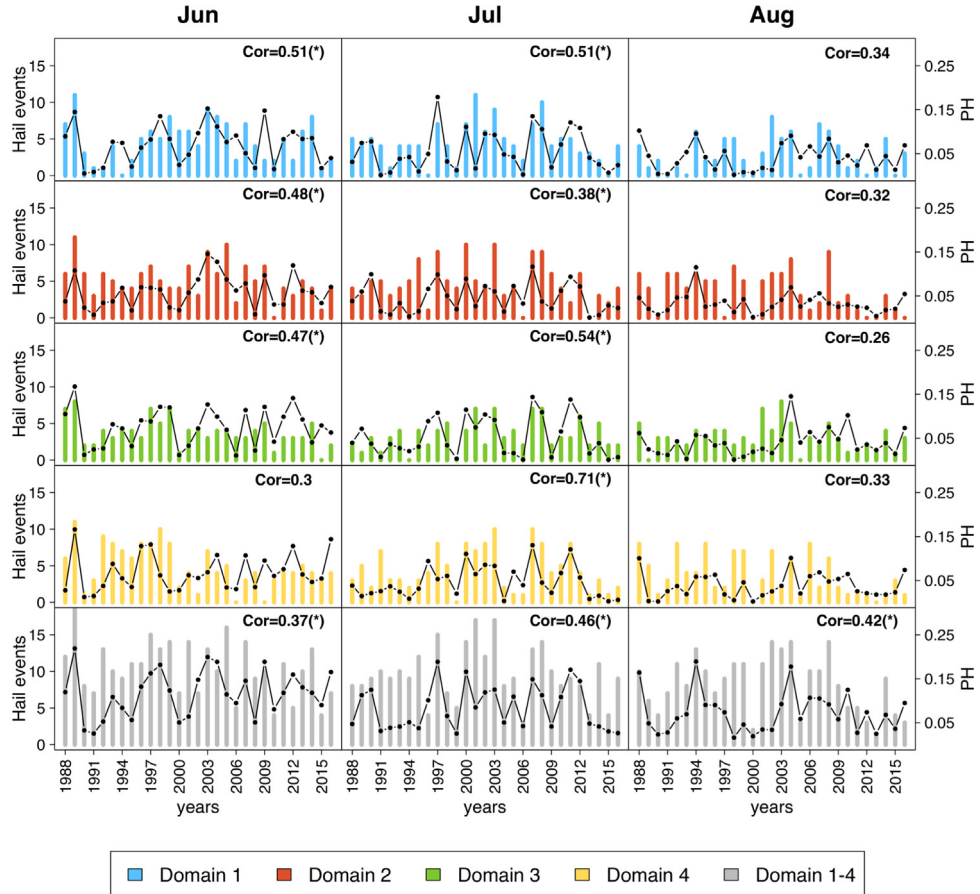


Fig. 8. Number of ARPA FVG hail events for every single month and year (bars) and the monthly mean of the GHM daily maximum PH (see Fig. 2a for the location of the domains). The correlation between the PH and the number of hail observations is shown in the top-right corner. Significant correlation values at the 95% confidence level are marked with an asterisk.

that the SHM is more sensitive to situations with high convective potential. Convective instability is typically higher over land during the warmest months when the solar heating near the surface is larger (Lolis, 2017; Holley et al., 2014). The rise of warm and humid air allows CAPE and the other convective indices to reach extreme values (Taszarek et al., 2018), and the PH increases accordingly. Moreover, CIN delays convective initiation so that the energy release (CAPE) is larger. Environments with high values of both CIN and CAPE are the most disruptive, as they are often associated with isolated supercells where large hail can develop (Calvo-Sancho et al., 2022; Taszarek et al., 2020). Indeed, the majority of the severe hail events occur in July and August and the SHM mostly relies on those data for calibration (Fig. 1d). Finally, the different vertical levels used for wind shear computation suggest that the SHM (which uses WSH03) is more affected by the smoothed orography issue than the GHM (WSH06), and this is another potential explanation for its scarce capability of reproducing hail potential on the mountains.

5.3. Influence of the GA selected predictors on the model output

As discussed in the previous section, the performance of the hail models depends on the set of predictors indicated by the GA. The discriminant power of a predictor can be gathered by the extent to which the climatological (black) and hail-conditioned (red) curves overlap in Fig. 4. CAPE is generally recognized as the best proxy for hail environments. For example, CAPE has shown the ability to discriminate between thunderstorms and thunderstorms with hail (Czernecki et al., 2019). In addition, CAPE is shown to be positively correlated with hailstone size (Taszarek et al., 2020). The hail-conditioned values of

CAPE obtained in this work are quite similar to other works focused on Europe (e.g., Taszarek et al., 2018; Brooks, 2009) whereas they are lower than those for the United States (Prein and Holland, 2018). Such differences reflect known regional dependencies of the hail environments (Allen et al., 2020; Taszarek et al., 2020). Beyond CAPE, wind shear is also considered a good candidate in several hail studies, from the surface to 3 km and surface to 6 km (Prein and Holland, 2018 and Brooks, 2009, respectively). For Europe, Taszarek et al. (2020) found that WSH03 (WSH06) exceeding 15(20) m/s is associated with severe weather. The peaks of hail-conditioned PDFs for WSH03 and WSH06 (Fig. 4i and f, respectively) equal those values. Regarding convective indices, standard choices are among those referenced in Mohr and Kunz (2013) and Kunz (2007). All the convective variables considered in Table 1 have been eventually selected, either in the GHM or in the SHM, or in both. The hail-conditioned values in Kunz (2007) for TOTALI and KI (referred to Germany) are slightly higher compared to 5. On the other hand, Manzato (2012) derived CIN values from soundings over the FVG region during hail episodes and found that $CIN > 50 \text{ J/K}$ maximizes the PSS for hail days' detection. This threshold equals the peak of the hail-conditioned PDF derived from ESWD observations, as shown in Fig. 5g. Finally, other typical hail predictors such as sounding-derived parameters, humidity and temperature parameters have been considered in the literature (Czernecki et al., 2019).

5.4. Validation approach and metrics

The GA selects the predictors according to the hail events that are used for calibration. Hail events are also needed to validate the model output and the choice of the calibration and validation datasets is

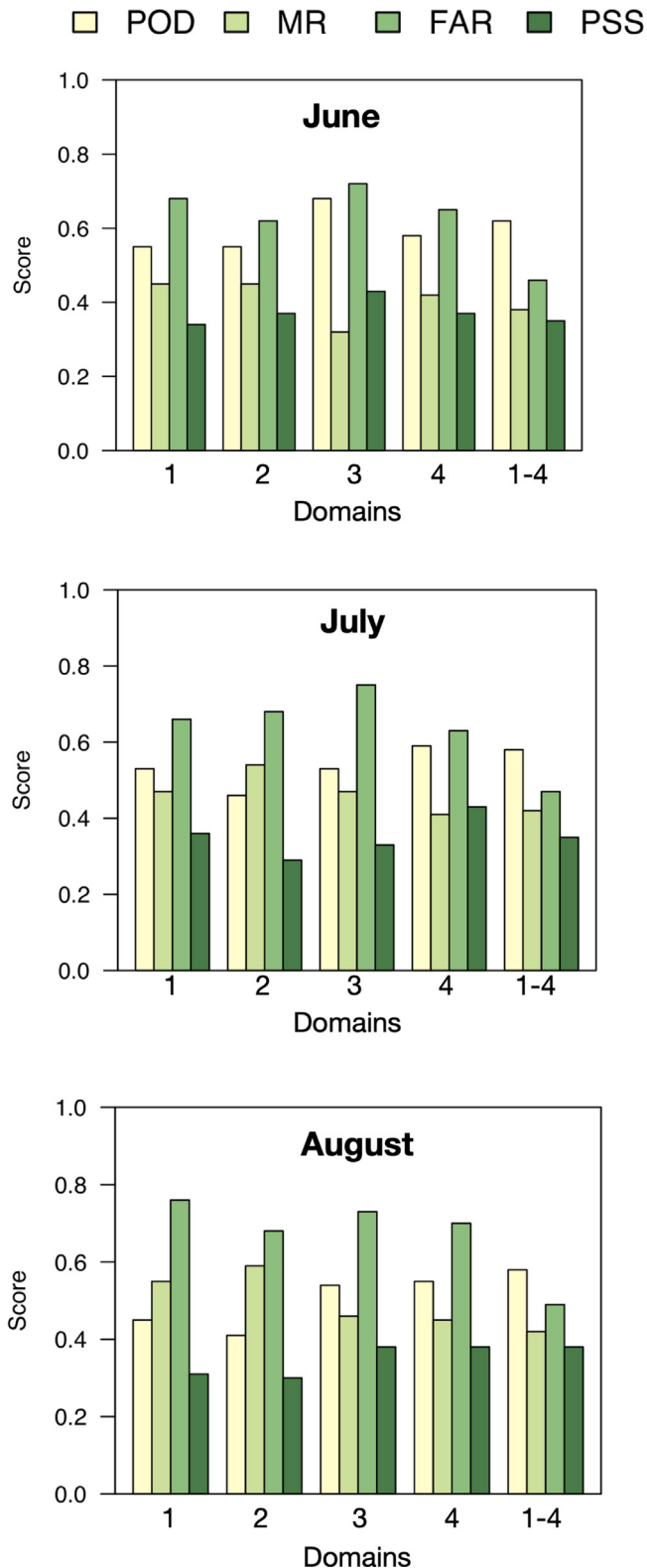


Fig. 9. Probability of detection (POD), Miss rate (MR), False Alarm Ratio (FAR) and Peirce Skill Score (PSS). The PH values from the GHM have been transformed into binary hail occurrences (a hail day is a day with a PH above the probability threshold of 0.0049). The ARPA FVG dataset is the observational reference. The scores have been computed for June, July and August in the 1988–2016 period.

a crucial one. In this work, two different observational hail datasets have been used. The ESWD reports served as input data for the GA whereas the ARPA FVG database has been used as a ground-based

reference for independent validation. Of course, the two datasets are complementary: the ESWD covers the 2000–2020 period (Fig. 1b), while the ARPA FVG dataset is available for 1988–2016 (Fig. 2b). The ESWD dataset is more suitable for calibration as it includes hail events spread over the whole country, thus it accounts for a certain variety of hail environmental conditions that are needed for the model to reproduce the hail variability in Italy. The accurate selection of non-hail days, as explained in Section 4.4, made this calibration dataset well-balanced. On the other hand, the ARPA FVG hail pads networks consist of an objective and homogeneous dataset of hail events, with good temporal continuity and a proper representation of hail and non-hail events (guaranteed by the hail pad measuring system) that is essential to compute performance metrics.

Several shortcomings related to the validation process have been identified in previous hail studies, especially in Italy. In the study of Ecel et al. (2012), ERA40 weather variables are considered over 6 grid points covering the entire NE of Italy (2.5° spatial resolution) although they are compared with very localized hail pad networks. Baldi et al. (2014) developed a country-wide study but results are aggregated on six climatic macro-regions, relating this to the lack of a nationwide hail monitoring system. Moreover, validation is performed only over FVG, by means of ARPA FVG data available at that time, albeit not shown in their manuscript. Therefore, the validation of a hail model for Italy over the FVG region shown in this work (Section 4.4) represents a considerable improvement with respect to the current information available for Italy.

At the European level, validation has been performed by means of a variety of independent data sources such as insurance claims and radar reflectivity (e.g., Madonna et al., 2018; Nisi et al., 2016; Mohr et al., 2015a) with very good spatial coverage. However, as for Italy, the output is aggregated over very large domains, either box of a certain size (100 × 100 km), climatic regions or countries. Despite this, the performance metrics rarely exceed those from the GHM presented here. For example, the correlation coefficient for the inter-annual variability of hail frequency in the GHM model scored up to 0.5 over the full FVG domain and even more for specific months and subdomains. Madonna et al. (2018) attained a correlation up to 0.8, although boxes are twice the size of the verification domains in FVG which have been used in this work. Allen et al. (2015) validate their model over large domains in the United States and the corresponding correlations score 0.5 on average, with specific over-performing months and regions. Typically, the best scores are attained during the hail peak months, when more data is available for verification.

The way the hail model is designed, that is estimating a hail occurrence based on the environmental conditions potentially favourable to its development, makes a certain over-prediction of hail events expected. Indeed, high FAR values are a well-known issue that has been already reported in similar works on severe storm environments (e.g., Czernecki et al., 2019; Allen et al., 2015; Mohr and Kunz, 2013; Allen et al., 2011; Kunz, 2007; Rasmussen and Blanchard, 1998). This is due to the difficulties associated with the detection of rare, localized and rapid events (e.g., hail), which make observations limited in size and poorly homogeneous. Hence, in practice, it is expected that both the POD and the FAR do not literally run from 0 to 1 (Hitchens et al., 2013). Over-prediction of a few events per year is observed in Prein and Holland (2018) although they do not provide specific verification metrics. The best POD (FAR) values obtained by the GHM, for the full FVG domain, are around 0.6 (0.45). This equals (improves) what, for example, Mohr et al. (2015b) and Czernecki et al. (2019) obtained for country-scale verification. In Pullman et al. (2019), the POD is around 0.5 but FAR lowers to ~ 0.3, with a verification domain comparable to FVG. However, the model is constructed with satellite data and does not suffer from observational biases. Finally, in Manzato (2012) both POD and FAR are higher and PSS is similar to what has been obtained by the GHM.

To sum up, the size increase of the verification domain may lead to better scores albeit it also reduces the quality and the usefulness of the hail hazard information. It is not straightforward to define an optimal size, and this should be done as a trade-off between the availability of data and the desired output accuracy.

6. Conclusions

Italy is one of the most exposed countries to the hail hazard in Europe. However, the scarcity of hail observational networks has prevented the systematic characterization of the hail conditions in this country. To overcome this limitation, large-scale atmospheric variables and convective indices can be used as predictors for the estimation of the hail probability. This concept has fostered some studies, mainly addressing very large domains that include different climate zones and environmental conditions for hail formation. The link between the large-scale ERA5 variables and the hail occurrences over Italy has been explored in the present study. This analysis identifies differences (in terms of values and temporal evolution) in the influence that specific atmospheric variables exert on hail events.

This work has exploited the large amount of information available in the ERA5 reanalysis to develop a model that provides long-term time series (1979–2020) of the hail probability over the Italian domain, with a spatial resolution of 30 km. Most of the hail models in the literature focus on severe hail events (typically defined as events with hailstone diameters exceeding 2 or 3 cm). These are similar to the SHM developed in the present study. An innovative aspect of this work is that a General Hail Model is also developed, trained with all the available hail observations, without any constraint on the hailstone size. The comparison with SHM is included to investigate the benefits and drawbacks of both approaches.

The developed models are inspired by a hail model currently available (Prein and Holland, 2018), with the goal of improving its flexibility and applicability by its integration with a genetic algorithm. The main advantage of the GA method is the systematic identification of the best set of predictors. However, these predictors might be different for specific set-ups (e.g., regions or observational datasets employed for calibration). In addition, this GA approach provides parameters such as the minimum PH threshold to define hail days, which are essential to establish the hail hazard in an objective way.

Results from both hail models have shown that the highest values of hail probability affect northern (southern) Italy in early (late) summer. Particularly, the GHM can be useful beyond the summer season (April, May and September) when the hail events are less frequent and typically weaker (Púćik et al., 2019), but also over mountain grid points. The results presented in this paper are provided with a higher spatial resolution (0.25° vs. 1°) with respect to Prein and Holland (2018) which allows a novel sub-regional assessment of hail hazard. The Prein and Holland (2018) model was originally developed for the United States and validated in Europe despite several limitations. Conversely, the GHM and SHM developed in this study have been designed and verified for Italy. Verification is performed for specific domains in the FVG region as the under-sampling of hail observations still represents a caveat. Performance metrics are satisfactory, especially for the summer months when most of the events occur. However, the hail models suffer from a certain degree of over-prediction, which is a common feature of similar probabilistic approaches.

Therefore, there is room for improvement for both the GHM and the SHM. First, an ideal calibration could be attained with a more homogeneous distribution of the training hail observations, compared to the ESWD data that has been used (Fig. 1). At the temporal scale, the number of hail reports has increased in recent years, thanks to a higher engagement of the volunteers. This is promising, as long-term observations are also crucial for a more robust model set-up. Second, the hail models could be further improved over mountain

grid points. At the current stage, one limitation comes from the effects of the ERA5 smoothed orography in the lowest model levels. Increasing the resolution of the reanalysis products would allow for a better representation of the atmospheric processes occurring over complex topography. Therefore, their use for the hail model would enable a more accurate characterization of the hail hazard over those areas. Since the Italian domain is largely characterized by complex orographic structures and land-sea margins, this is a crucial aspect to boost the applicability of the hail model towards the sub-regional scale. Reanalysis data with higher spatial resolutions than ERA5 such as MERIDA (Bonanno et al., 2019) and ERA5-Land (Muñoz Sabater et al., 2021) are currently available, but the use of these datasets is not straightforward as they do not have sufficient temporal coverage and the output atmospheric variables are quite limited.

The future work will cover the historical analysis of hail hazard over the past decades, including the trend computation for the predictors so that their relative contributions can be assessed. Finally, a further effort will be devoted to the implementation of this methodology into operational weather forecasts, that provide for an exhaustive set of atmospheric variables. This would allow the production of hail forecasts and exploration of future hail variability on multiple time ranges, including the seasonal, decadal, and climate change scenarios perspectives.

CRediT authorship contribution statement

Verónica Torralba: Conceptualization, Data curation, Formal analysis, Methodology, Writing – original draft, Writing – review. **Riccardo Hénin:** conceptualization, data curation, Formal analysis, Methodology, Writing – original draft, Writing – review. **Antonio Cantelli:** conceptualization, Methodology, Software, Data curation. **Enrico Scoccimarro:** Writing – original draft, Review, Methodology. **Stefano Materia:** Writing – original draft, Review, Methodology. **Agostino Manzato:** Writing – original draft, Review, Data curation, Methodology. **Silvio Gualdi:** Writing – original draft, Review, Methodology.

Declaration of competing interest

The authors declare that they have no known competing financial interests or personal relationships that could have appeared to influence the work reported in this paper.

Data availability

Data will be made available on request.

Acknowledgements

The authors would like to thank the European Severe Storms Laboratory (ESSL) team for providing the hail data available in the European Severe Weather Database (ESWD). We also acknowledge the ECMWF for producing the ERA5 reanalysis under the Copernicus Climate Change program. Finally, we want to thank all the volunteers of the Friuli Venezia Giulia hail pad network and the team of OSMER - ARPA FVG (in particular Andrea Cicogna and Massimo Centore) for the collection and processing of the hail pad data.

Appendix A. Supplementary data

Supplementary material related to this article can be found online at <https://doi.org/10.1016/j.wace.2022.100535>.

References

- Allen, J.T., Giannanco, I.M., Kumjian, M.R., Punge, H.J., Zhang, Q., Groenemeijer, P., Kunz, M., Ortega, K., 2020. Understanding hail in the earth system. *Rev. Geophys.* 58, <http://dx.doi.org/10.1029/2019RG000665>.
- Allen, J.T., Karoly, D.J., Mills, G.A., 2011. A severe thunderstorm climatology for Australia and associated thunderstorm environments. *Aust. Meteorol. Oceanogr. J.* 61 (3), 143. <http://dx.doi.org/10.22499/2.6103.001>.
- Allen, J.T., Tippett, M.K., Sobel, A.H., 2015. An empirical model relating U.S. monthly hail occurrence to large-scale meteorological environment. *J. Adv. Modelling Earth Syst.* 7, <http://dx.doi.org/10.1002/2014MS000397>.
- Baiamonte, I., Raffo, A., Nardo, N., Moneta, E., Peparaio, M., D'Aloise, A., Kelderer, M., Casera, C., Paoletti, F., 2016. Effect of the use of anti-hail nets on codling moth (*Cydia pomonella*) and organoleptic quality of apple (cv. Braeburn) grown in Alto Adige Region (northern Italy). *J. Sci. Food Agric.* 96 (6), 2025–2032. <http://dx.doi.org/10.1002/jsfa.7313>.
- Baldi, M., Ciardini, V., Dalu, J.D., De Filippis, T., Maracchi, G., Dalu, G., 2014. Hail occurrence in Italy: Towards a national database and climatology. *Atmos. Res.* 138, 268–277. <http://dx.doi.org/10.1016/j.atmosres.2013.11.012>.
- Bonanno, R., Lacavalla, M., Sperati, S., 2019. A new high-resolution meteorological reanalysis Italian dataset: MERIDA. *Q. J. R. Meteorol. Soc.* 145 (721), 1756–1779. <http://dx.doi.org/10.1002/qj.3530>.
- Boughorbel, S., Jaray, F., El-Albari, M., 2017. Optimal classifier for imbalanced data using matthews correlation coefficient metric. *PLoS One* 12 (6), e0177678. <http://dx.doi.org/10.1371/journal.pone.0177678>.
- Brooks, H.E., 2009. Proximity soundings for severe convection for Europe and the United States from reanalysis data. *Atmos. Res.* 93 (1), 546–553. <http://dx.doi.org/10.1016/j.atmosres.2008.10.005>, 4th European Conference on Severe Storms.
- Brooks, H.E., Lee, J.W., Craven, J.P., 2003. The spatial distribution of severe thunderstorm and tornado environments from global reanalysis data. *Atmos. Res.* 67, 73–94. [http://dx.doi.org/10.1016/S0169-8095\(03\)00045-0](http://dx.doi.org/10.1016/S0169-8095(03)00045-0).
- Brown, T.M., Pogorzelski, W.H., Giannanco, I.M., 2015. Evaluating hail damage using property insurance claims data. *Weather Clim. Soc.* 7 (3), 197–210. <http://dx.doi.org/10.1175/WCAS-D-15-0011.1>.
- Bunkers, M.J., Klimowski, B.A., Zeitzer, J.W., Thompson, R.L., Weisman, M.L., 2000. Predicting supercell motion using a new hodograph technique. *Weather Forecast.* 15 (1), 61–79. [http://dx.doi.org/10.1175/1520-0434\(2000\)015<0061:PSMUAN>2.0.CO;2](http://dx.doi.org/10.1175/1520-0434(2000)015<0061:PSMUAN>2.0.CO;2).
- Calvo-Sancho, C., Díaz-Fernández, J., Martín, Y., Bolgiani, P., Sastre, M., González-Alemán, J.J., Santos-Muñoz, D., Farrán, J.I., Martín, M.L., 2022. Supercell convective environments in Spain based on ERA5: hail and non-hail differences. *Weather Clim. Dyn.* 3 (3), 1021–1036. <http://dx.doi.org/10.5194/wcd-3-1021-2022>.
- Changnon, S.A., Changnon, D., Hilberg, S.D., 2009. Hailstorms across the nation: An atlas about hail and its damages. URL: <https://www.ideals.illinois.edu/handle/2142/15156>.
- Chicco, D., Jurman, G., 2020. The advantages of the matthews correlation coefficient (MCC) over F1 score and accuracy in binary classification evaluation. *BMC Genom.* 21 (1), 1–13. <http://dx.doi.org/10.1186/s12864-019-6413-7>.
- Chicco, D., Tötsch, N., Jurman, G., 2021. The matthews correlation coefficient (MCC) is more reliable than balanced accuracy, bookmaker informedness, and markedness in two-class confusion matrix evaluation. *BioData Min.* 14 (1), 1–22. <http://dx.doi.org/10.1186/s13040-021-00244-z>.
- Czernecki, B., Taszarek, M., Marosz, M., Pórolniczak, M., Kolendowicz, L., Wyszogrodzki, A., Szturc, J., 2019. Application of machine learning to large hail prediction - The importance of radar reflectivity, lightning occurrence and convective parameters derived from ERA5. *Atmos. Res.* 227, <http://dx.doi.org/10.1016/j.atmosres.2019.05.010>.
- Dessens, J., Fraile, R., 1994. Hailstone size distributions in southwestern France. *Atmos. Res.* 33 (1–4), 57–73. [http://dx.doi.org/10.1016/0169-8095\(94\)90013-2](http://dx.doi.org/10.1016/0169-8095(94)90013-2).
- Dixon, M., Wiener, G., 1993. TITAN: Thunderstorm identification, tracking, analysis, and nowcasting—A radar-based methodology. *J. Atmos. Ocean. Technol.* 10 (6), 785–797. [http://dx.doi.org/10.1175/1520-0426\(1993\)010<0785:TITAA>2.0.CO;2](http://dx.doi.org/10.1175/1520-0426(1993)010<0785:TITAA>2.0.CO;2).
- Dotzek, N., Groenemeijer, P., Feuerstein, B., Holzer, A.M., 2009. Overview of ESSL's severe convective storms research using the European severe weather database ESWD. *Atmos. Res.* 93, <http://dx.doi.org/10.1016/j.atmosres.2008.10.020>.
- Eccel, E., Cau, P., Riemann-Campe, K., Biasioli, F., 2012. Quantitative hail monitoring in an alpine area: 35-year climatology and links with atmospheric variables. *Int. J. Climatol.* 32, <http://dx.doi.org/10.1002/joc.2291>.
- Fernández, A., García, S., Galar, M., Prati, R.C., Krawczyk, B., Herrera, F., 2018. Learning from Imbalanced Data Sets, Vol. 10. Springer.
- Fluck, E., Kunz, M., Geissbuehler, P., Ritz, S.P., 2021. Radar-based assessment of hail frequency in Europe. *Nat. Hazards Earth Syst. Sci.* 21 (2), 683–701. <http://dx.doi.org/10.5194/nhess-21-683-2021>.
- Gagne, D.J., McGovern, A., Haupt, S.E., Sobash, R.A., Williams, J.K., Xue, M., 2017. Storm-based probabilistic hail forecasting with machine learning applied to convection-allowing ensembles. *Weather Forecast.* 32 (5), 1819–1840. <http://dx.doi.org/10.1175/WAF-D-17-0010.1>.
- García-Ortega, E., López, L., Sánchez, J., 2011. Atmospheric patterns associated with hailstorm days in the Ebro Valley, Spain. *Atmos. Res.* 100 (4), 401–427. <http://dx.doi.org/10.1016/j.atmosres.2010.08.023>.
- Giaiotti, D., Giancesini, E., Stel, F., 2001. Heuristic considerations pertaining to hailstone size distributions in the plain of Friuli-Venezia Giulia. *Atmos. Res.* 57 (4), 269–288. [http://dx.doi.org/10.1016/S0169-8095\(01\)00080-1](http://dx.doi.org/10.1016/S0169-8095(01)00080-1).
- Giaiotti, D., Nordio, S., Stel, F., 2003. The climatology of hail in the plain of Friuli Venezia Giulia. *Atmos. Res.* 67, 247–259. [http://dx.doi.org/10.1016/S0169-8095\(03\)00084-X](http://dx.doi.org/10.1016/S0169-8095(03)00084-X).
- Goldberg, D.E., Holland, J.H., 1988. *Genetic algorithms and machine learning*. Groenemeijer, P., Púčik, T., Holzer, A.M., Antonescu, B., Riemann-Campe, K., Schultz, D.M., Kühne, T., Feuerstein, B., Brooks, H.E., Doswell III, C.A., et al., 2017. Severe convective storms in Europe: Ten years of research and education at the European severe storms laboratory. *Bull. Am. Meteorol. Soc.* 98, <http://dx.doi.org/10.1175/BAMS-D-16-0067.1>.
- Hassanat, A., Almohammadi, K., Alkfaween, E., Abunawas, E., Hammouri, A., Prasath, V.S., 2019. Choosing mutation and crossover ratios for genetic algorithms—a review with a new dynamic approach. *Information* 10 (12), 390. <http://dx.doi.org/10.3390/info10120390>.
- Haupt, R.L., Haupt, S.E., 2004. *Practical Genetic Algorithms*. John Wiley & Sons.
- Hersbach, H., Bell, B., Berrisford, P., Hirahara, S., Horányi, A., Muñoz-Sabater, J., Nicolas, J., Peubey, C., Radu, R., Schepers, D., Simmons, A., Soci, C., Abdalla, S., Abellan, X., Balsamo, G., Bechtold, P., Biavati, G., Bidlot, J., Bonavita, M., Chiara, G., Dahlgren, P., Dee, D., Diamantakis, M., Dragani, R., Flemming, J., Forbes, R., Fuentes, M., Geer, A., Haimberger, L., Healy, S., Hogan, R.J., Hólm, E., Janisková, M., Keeley, S., Laloyaux, P., Lopez, P., Lupu, C., Radnoti, G., Rosnay, P., Rozum, I., Vamborg, F., Villaume, S., Thépaut, J.-N., 2020. The ERA5 global reanalysis. *Q. J. R. Meteorol. Soc.* 146, <http://dx.doi.org/10.1002/qj.3803>.
- Hitchens, N.M., Brooks, H.E., Kay, M.P., 2013. Objective limits on forecasting skill of rare events. *Weather Forecast.* 28 (2), 525–534. <http://dx.doi.org/10.1175/WAF-D-12-00113.1>.
- Holley, D.M., Dorling, S.R., Steele, C.J., Earl, N., 2014. A climatology of convective available potential energy in great britain. *Int. J. Climatol.* 34 (14), 3811–3824. <http://dx.doi.org/10.1002/joc.3976>.
- Jelić, D., Megyeri, O.A., Malečić, B., Belušić Vozila, A., Strelec Mahović, N., Telišman Prtenjak, M., 2020. Hail climatology along the northeastern Adriatic. *J. Geophys. Res.: Atmos.* 125 (23), e2020JD032749. <http://dx.doi.org/10.1029/2020JD032749>.
- Jolliffe, I.T., Stephenson, D.B., 2012. *Forecast Verification: A Practitioner's Guide in Atmospheric Science*. John Wiley & Sons.
- Katoch, S., Chauhan, S.S., Kumar, V., 2021. A review on genetic algorithm: past, present, and future. *Multimedia Tools Appl.* 80 (5), 8091–8126. <http://dx.doi.org/10.1007/s11042-020-10139-6>.
- Kelley, C., Ting, M., Seager, R., Kushnir, Y., 2012. Mediterranean precipitation climatology, seasonal cycle, and trend as simulated by CMIP5. *Geophys. Res. Lett.* 39 (21), <http://dx.doi.org/10.1029/2012GL053416>.
- Khodayar, S., Kalthoff, N., Kottmeier, C., 2016. Atmospheric conditions associated with heavy precipitation events in comparison to seasonal means in the western mediterranean region. *Clim. Dynam.* 51, 951–967. <http://dx.doi.org/10.1007/s00382-016-3058-y>.
- Krawczyk, B., 2016. Learning from imbalanced data: open challenges and future directions. *Prog. Artif. Intell.* 5, 221–232. <http://dx.doi.org/10.1007/s13748-016-0094-0>.
- Kunz, M., 2007. The skill of convective parameters and indices to predict isolated and severe thunderstorms. *Nat. Hazards Earth Syst. Sci.* 7 (2), 327–342. <http://dx.doi.org/10.5194/nhess-7-327-2007>.
- Kunz, M., Wandel, J., Fluck, E., Baumstark, S., Mohr, S., Schemm, S., 2020. Ambient conditions prevailing during hail events in central Europe. *Nat. Hazards Earth Syst. Sci.* 20 (6), 1867–1887. <http://dx.doi.org/10.5194/nhess-20-1867-2020>.
- Laviola, S., Levizzani, V., Ferraro, R.R., Beauchamp, J., 2020. Hailstorm detection by satellite microwave radiometers. *Remote Sens.* 12 (4), 621. <http://dx.doi.org/10.3390/rs12040621>.
- Lionello, P., Trigo, I.F., Gil, V., Liberato, M.L.R., Nissen, K.M., Pinto, J.G., Raible, C.C., Reale, M., Tanzarella, A., Trigo, R.M., Ulbrich, S., Ulbrich, U., 2016. Objective climatology of cyclones in the mediterranean region: a consensus view among methods with different system identification and tracking criteria. *Tellus A: Dyn. Meteorol. Oceanogr.* 68 (1), 29391. <http://dx.doi.org/10.3402/tellusa.v68.29391>.
- Lolis, C.J., 2017. A climatology of convective available potential energy in the mediterranean region. *Clim. Res.* 74 (1), 15–30, URL: <https://www.jstor.org/stable/26394473>.
- Macdonald, H., Infield, D., Nash, D.H., Stack, M.M., 2016. Mapping hail meteorological observations for prediction of erosion in wind turbines. *Wind Energy* 19, <http://dx.doi.org/10.1002/we.1854>.
- Madonna, E., Ginsbürger, D., Martius, O., 2018. A Poisson regression approach to model monthly hail occurrence in northern Switzerland using large-scale environmental variables. *Atmos. Res.* 203, <http://dx.doi.org/10.1016/j.atmosres.2017.11.024>.
- Manzato, A., 2012. Hail in northeast Italy: Climatology and bivariate analysis with the sounding-derived indices. *J. Appl. Meteorol. Climatol.* 51 (3), 449–467. <http://dx.doi.org/10.1175/JAMC-D-10-05012.1>.

- Manzato, A., 2013. Hail in northeast Italy: A neural network ensemble forecast using sounding-derived indices. *Weather Forecast.* 28 (1), 3–28. <http://dx.doi.org/10.1175/WAF-D-12-00034.1>.
- Manzato, A., Cicogna, A., Centore, M., Battistutta, P., Trevisan, M., 2022a. Hailstone characteristics in NE Italy from 29 years of hailpad data. *J. Appl. Meteorology Climatology* 61 (11), 1779–1795. <http://dx.doi.org/10.1175/JAMC-D-21-0251.1>.
- Manzato, A., Riva, V., Tiesi, A., Marcello Miglietta, M., 2020. Observational analysis and simulations of a severe hailstorm in northeastern Italy. *Q. J. R. Meteorol. Soc.* 146 (732), 3587–3611. <http://dx.doi.org/10.1002/qj.3886>.
- Manzato, A., Serafin, S., Miglietta, M.M., Kirshbaum, D., Schulz, W., 2022b. A pan-alpine climatology of lightning and convective initiation. *Mon. Weather Rev.* <http://dx.doi.org/10.1175/MWR-D-21-0149.1>.
- Markowski, P.M., Dotzek, N., 2011. A numerical study of the effects of orography on supercells. *Atmos. Res.* 100 (4), 457–478. <http://dx.doi.org/10.1016/j.atmosres.2010.12.027>, 5th European Conference on Severe Storms.
- Marra, A., Porcù, F., Baldini, L., Petracca, M., Casella, D., Dietrich, S., Mugnai, A., Sanò, P., Vulpiani, G., Panegrossi, G., 2017. Observational analysis of an exceptionally intense hailstorm over the mediterranean area: Role of the GPM core observatory. *Atmos. Res.* 192, 72–90. <http://dx.doi.org/10.1016/j.atmosres.2017.03.019>.
- Martius, O., Hering, A., Kunz, M., Manzato, A., Mohr, S., Nisi, L., Trefalt, S., 2018. Challenges and recent advances in hail research. *Bull. Am. Meteorol. Soc.* 99, <http://dx.doi.org/10.1175/BAMS-D-17-0207.1>.
- Marzban, C., Witt, A., 2001. A Bayesian neural network for severe-hail size prediction. *Weather Forecast.* 16 (5), 600–610. [http://dx.doi.org/10.1175/1520-0434\(2001\)016<0600:ABNNFS>2.0.CO;2](http://dx.doi.org/10.1175/1520-0434(2001)016<0600:ABNNFS>2.0.CO;2).
- Materia, S., Muñoz, Á.G., Álvarez-Castro, M.C., Mason, S.J., Vitart, F., Gualdi, S., 2020. Multimodel subseasonal forecasts of spring cold spells: Potential value for the hazelnut agribusiness. *Weather Forecast.* 35 (1), 237–254.
- Merino, A., Sánchez, J., Fernández-González, S., García-Ortega, E., Marcos, J., Berthet, C., Dessens, J., 2019. Hailfalls in southwest Europe: EOF analysis for identifying synoptic pattern and their trends. *Atmos. Res.* 215, 42–56. <http://dx.doi.org/10.1016/j.atmosres.2018.08.006>.
- Mills, K.L., Filliben, J.J., Haines, A.L., 2015. Determining relative importance and effective settings for genetic algorithm control parameters. *Evol. Comput.* 23 (2), 309–342. http://dx.doi.org/10.1162/EVCO_a_00137.
- Mitchell, M., 1998. An introduction to genetic algorithms.
- Mohr, S., Kunz, M., 2013. Recent trends and variabilities of convective parameters relevant for hail events in Germany and Europe. *Atmos. Res.* 123, <http://dx.doi.org/10.1016/j.atmosres.2012.05.016>.
- Mohr, S., Kunz, M., Geyer, B., 2015b. Hail potential in Europe based on a regional climate model hindcast. *Geophys. Res. Lett.* 42, <http://dx.doi.org/10.1002/2015GL067118>.
- Mohr, S., Kunz, M., Keuler, K., 2015a. Development and application of a logistic model to estimate the past and future hail potential in Germany. *J. Geophys. Res.: Atmos.* 120 (9), 3939–3956. <http://dx.doi.org/10.1002/2014JD022959>.
- Montopoli, M., Picciotti, E., Baldini, L., Di Fabio, S., Marzano, F., Vulpiani, G., 2021. Gazing inside a giant-hail-bearing mediterranean supercell by dual-polarization Doppler weather radar. *Atmos. Res.* 264, 105852. <http://dx.doi.org/10.1016/j.atmosres.2021.105852>.
- Muehleisen, W., Eder, G.C., Voronko, Y., Spielberger, M., Sonnleitner, H., Knoebel, K., Ebner, R., Ujvari, G., Hirschl, C., 2018. Outdoor detection and visualization of hailstorm damages of photovoltaic plants. *Renew. Energy* 118, 138–145. <http://dx.doi.org/10.1016/j.renene.2017.11.010>.
- Muñoz Sabater, J., Dutra, E., Agustí-Panareda, A., Albergel, C., Arduini, G., Balsamo, G., Boussetta, S., Choulga, M., Harrigan, S., Hersbach, H., Martens, B., Miralles, D.G., Piles, M., Rodríguez-Fernández, N.J., Zsoter, E., Buontempo, C., Thépaut, J.-N., 2021. ERA5-land: a state-of-the-art global reanalysis dataset for land applications. *Earth Syst. Sci. Data* 13 (9), 4349–4383. <http://dx.doi.org/10.5194/essd-13-4349-2021>.
- Nisi, L., Martius, O., Hering, A., Kunz, M., Germann, U., 2016. Spatial and temporal distribution of hailstorms in the Alpine region: a long-term, high resolution, radar-based analysis. *Q. J. R. Meteorol. Soc.* 142 (697), 1590–1604. <http://dx.doi.org/10.1002/qj.2771>.
- Palencia, C., Castro, A., Giacinti, D., Stel, F., Vinet, F., Fraile, R., 2009. Hailpad-based research: A bibliometric review. *Atmos. Res.* 93 (1–3), 664–670. <http://dx.doi.org/10.1016/j.atmosres.2008.09.025>.
- Peirce, C.S., 1884. The numerical measure of the success of predictions. *Science* (93), 453–454. <http://dx.doi.org/10.1126/science.ns-4.93.453.b>.
- Piani, F., Crisci, A., De Chiara, G., Maracchi, G., Meneguzzo, F., 2005. Recent trends and climatic perspectives of hailstorms frequency and intensity in Tuscany and central Italy. *Nat. Hazards Earth Syst. Sci.* 5 (2), 217–224. <http://dx.doi.org/10.5194/nhess-5-217-2005>.
- Prein, A.F., Holland, G.J., 2018. Global estimates of damaging hail hazard. *Weather Clim. Extremes* 22, 10–23. <http://dx.doi.org/10.1016/j.wace.2018.10.004>.
- Púčik, T., Castellano, C., Groenemeijer, P., Kühne, T., Rädler, A.T., Antonescu, B., Faust, E., 2019. Large hail incidence and its economic and societal impacts across Europe. *Mon. Weather Rev.* 147 (11), 3901–3916. <http://dx.doi.org/10.1175/MWR-D-19-0204.1>.
- Pullman, M., Gurung, I., Maskey, M., Ramachandran, R., Christopher, S.A., 2019. Applying deep learning to hail detection: A case study. *IEEE Trans. Geosci. Remote Sens.* 57, <http://dx.doi.org/10.1109/TGRS.2019.2931944>.
- Punge, H., Bedka, K., Kunz, M., Reinbold, A., 2017. Hail frequency estimation across Europe based on a combination of overshooting top detections and the ERA-interim reanalysis. *Atmos. Res.* 198, <http://dx.doi.org/10.1016/j.atmosres.2017.07.025>.
- Punge, H.J., Bedka, K.M., Kunz, M., Werner, A., 2014. A new physically based stochastic event catalog for hail in Europe. *Nat. Hazards* 73, 1625–1645.
- Punge, H., Kunz, M., 2016. Hail observations and hailstorm characteristics in Europe: A review. *Atmos. Res.* 176–177, <http://dx.doi.org/10.1016/j.atmosres.2016.02.012>.
- Rasmussen, E.N., Blanchard, D.O., 1998. A baseline climatology of sounding-derived supercell and tornado forecast parameters. *Weather Forecast.* 13 (4), 1148–1164. [http://dx.doi.org/10.1175/1520-0434\(1998\)013<1148:ABCSD>2.0.CO;2](http://dx.doi.org/10.1175/1520-0434(1998)013<1148:ABCSD>2.0.CO;2).
- Raupach, T.H., Martius, O., Allen, J.T., Kunz, M., Lasher-Trapp, S., Mohr, S., Rasmussen, K.L., Trapp, R.J., Zhang, Q., 2021. The effects of climate change on hailstorms. *Nature Rev. Earth Environ.* <http://dx.doi.org/10.1038/s43017-020-00133-9>, 12.11.35; LK 01.
- Rivera, J.A., Otero, F., Naranjo Tamayo, E., Silva, M., 2020. Sixty years of hail suppression activities in Mendoza, Argentina: Uncertainties, gaps in knowledge and future perspectives. *Front. Environ. Sci.* 8, <http://dx.doi.org/10.3389/fenvs.2020.00045>.
- Roberto, N., Adirosi, E., Baldini, L., Casella, D., Dietrich, S., Gatlin, P., Panegrossi, G., Petracca, M., Sanò, P., Tokay, A., 2016. Multi-sensor analysis of convective activity in central Italy during the HyMeX SOP 1.1. *Atmos. Meas. Tech.* 9 (2), 535–552. <http://dx.doi.org/10.5194/amt-9-535-2016>.
- Rogna, M., Schamel, G., Weissensteiner, A., 2021. The apple producers' choice between hail insurance and anti-hail nets. *Agric. Finance Rev.* (25.06), <http://dx.doi.org/10.1108/afr-08-2020-0131>.
- Sánchez, J.L., Fraile, R., de la Madrid, J.L., de la Fuente, M.T., Rodríguez, P., Castro, A., 1996. Crop damage: The hail size factor. *J. Appl. Meteorol.* 35, [http://dx.doi.org/10.1175/1520-0450\(1996\)035<1535:CDTHSF>2.0.CO;2](http://dx.doi.org/10.1175/1520-0450(1996)035<1535:CDTHSF>2.0.CO;2).
- Santos, J.A., Belo-Pereira, M., 2019. A comprehensive analysis of hail events in Portugal: Climatology and consistency with atmospheric circulation. *Int. J. Climatol.* 39, <http://dx.doi.org/10.1002/joc.5794>.
- Tang, B.H., Gensini, V.A., Homeyer, C.R., 2019. Trends in United States large hail environments and observations. *Npj Clim. Atmosp. Sci.* 2, <http://dx.doi.org/10.1038/s41612-019-0103-7>.
- Taszarek, M., Allen, J.T., Púčik, T., Hoogewind, K.A., Brooks, H.E., 2020. Severe convective storms across Europe and the United States. Part II: ERA5 environments associated with lightning, large hail, severe wind, and tornadoes. *J. Clim.* 33 (23), 10263–10286. <http://dx.doi.org/10.1175/JCLI-D-20-0346.1>.
- Taszarek, M., Brooks, H.E., Czernecki, B., Szuster, P., Fortuniak, K., 2018. Climatological aspects of convective parameters over Europe: A comparison of ERA-interim and sounding data. *J. Clim.* 31 (11), 4281–4308. <http://dx.doi.org/10.1175/JCLI-D-17-0596.1>.
- Teule, T., Appeldorn, M., Bosma, P., Sprenger, L., Koks, E., de Moel, H., 2019. The Vulnerability of Solar Panels to Hail. *Water and Climate Risk*.
- Vulpiani, G., Baldini, L., Roberto, N., 2015. Characterization of mediterranean hail-bearing storms using an operational polarimetric X-band radar. *Atmos. Meas. Tech.* 8 (11), 4681–4698. <http://dx.doi.org/10.5194/amt-8-4681-2015>.
- Wilks, D.S., 2011. Statistical Methods in the Atmospheric Sciences, Vol. 100. Academic Press.